# OPTIMIZATION OF OPERATION TEMPERATURES AND DURATIONS DURING SOLAR THERMAL WATER SPLITTING TOWARDS GREATER ENERGY EFFICIENCIES

A THESIS SUBMITTED TO
THE GRADUATE SCHOOL OF NATURE AND APPLIED SCIENCES
OF
MIDDLE EAST TECHNICAL UNIVERSITY

BY

EZGİ YAVUZYILMAZ

IN PARTIAL FULFILLMENT OF THE REQUIREMENTS
FOR
THE DEGREE OF MASTER OF SCIENCE
IN
THE DEPARTMENT OF CHEMICAL ENGINEERING

SEPTEMBER 2016

Approval of the thesis:

**OPTIMIZATION OF OPERATION TEMPERATURES AND DURATIONS DURING SOLAR THERMAL WATER SPLITTING TOWARDS GREATER ENERGY EFFICIENCIES**

submitted by **EZGİ YAVUZYILMAZ** in partial fulfillment of the requirements for the degree of **Master of Science in Chemical Engineering Department, Middle East Technical University** by,

Prof. Dr. Gülbin Dural Ünver
Dean, Graduate School of **Natural and Applied Sciences** _____

Prof. Dr. Halil Kalıpçılar
Head of Department, **Chemical Engineering** _____

Prof. Dr. Deniz Üner
Supervisor, **Chemical Engineering Dept., METU** _____

Assoc. Prof. Dr. Serkan Kıncal
Co-Supervisor, **Chemical Engineering Dept., METU** _____

**Examining Committee Members:**

Prof. Dr. Derek K. Baker
Mechanical Engineering Dept., METU _____

Prof. Dr. Deniz Üner
Chemical Engineering Dept., METU _____

Assoc. Prof. Dr. Serkan Kıncal
Chemical Engineering Dept., METU _____

Assoc. Prof. Dr. N. Alper Tapan
Chemical Engineering Dept., Gazi University _____

Asst. Prof. Dr. Harun Koku
Chemical Engineering Dept., METU _____

**Date:** 07.09.2016

**I hereby declare that all information in this document has been obtained and presented in accordance with academic rules and ethical conduct. I also declare that, as required by these rules and conduct, I have fully cited and referenced all material and results that are not original to this work.**

Name, Last name : Ezgi Yavuzyılmaz

Signature :

## ABSTRACT

### OPTIMIZATION OF OPERATION TEMPERATURES AND DURATIONS DURING SOLAR THERMAL WATER SPLITTING TOWARDS GREATER ENERGY EFFICIENCIES

Yavuzyılmaz, Ezgi
M.S., Department of Chemical Engineering
Supervisor: Prof. Dr. Deniz Üner
Co-Supervisor: Assoc. Prof. Dr. Serkan Kıncal

September 2016, 95 Pages

Hydrogen production by solar thermal water splitting is an eco-friendly way of storing solar energy in chemical bonds. The most important obstacles for the viability and the commercialization of this technology are lower energy efficiencies and higher production costs compared to conventional hydrogen production ways such as steam reforming, coal gasification, and electrolysis of water.

Two-step thermochemical hydrogen production by using solar energy is an alternative method to conventional hydrogen production. In this method, the thermochemical cycle consists of two sequential steps: a high temperature step where the decomposition of the redox material is driven by solar energy and a relatively moderate temperature step where oxidation of the redox material is achieved by steam fed to the reactor. However, the changes in operation temperatures and process durations lead to trade-offs between performance criteria of the reactor. Therefore, the problem of evaluating optimum values for the operation temperatures and

durations have extreme significance in terms of achieving high energy efficiencies in the reactor.

In this thesis, more than one solution approach is presented for the solution of the problem. Both parametric statistical analysis approach and mathematical optimization methods are adopted to find local optima for operation temperatures and durations. Several local optimum values are presented for the studied specific reactor conditions and alternative cases.

**Keywords:** Solar hydrogen production, thermochemical, mathematical modeling, optimization

# ÖZ

## GÜNEŞ ENERJİSİ KULLANILARAK SUYUN BİLEŞENLERİNE AYRIŞTIRILMASINDA YÜKSEK ENERJİ VERİMLİLİĞİNE YÖNELİK PROSES SICAKLIK VE SÜRELERİNİN OPTİMİZASYONU

Yavuzyılmaz, Ezgi
Yüksek Lisans, Kimya Mühendisliği Bölümü
Tez Yöneticisi: Prof. Dr. Deniz Üner
Ortak Tez Yöneticisi: Doç. Dr. Serkan Kıncal

Eylül 2016, 95 Sayfa

Güneş enerjisi kullanılarak hidrojen üretimi, kimyasal bağlarda enerji depolanmasının çevreci, alternatif bir yoludur. Bu teknolojinin günümüzde yaygın bir biçimde kullanılmasını engelleyen en önemli problemler, buhar reformasyonu, kömürün gazlaştırılması ve suyun hidrolizi gibi geleneksel hidrojen üretim yöntemleri ile kıyaslandığında, bu teknolojinin düşük enerji verimliliği ve yüksek üretim maliyetlerine sahip olmasıdır.

Güneş enerjisi kullanarak suyun bileşenlerine ayrıştırılması önemli bir alternatif yöntemdir. Bu yöntemde, termokimyasal çevrim birbirini takip eden iki aşamadan oluşur. İlk aşamada, yüksek sıcaklıklarda redoks maddesi güneş enerjisinin yardımıyla ayrışır. İkinci aşamada ise görece düşük sıcaklıklarda su buharının reaktörden geçirilmesi ile redoks maddesinin yükseltgenmesi gerçekleşir. Ancak, çalışma sıcaklıkları ve sürelerindeki değişimler reaktörün birçok performans kriterleri arasında kar-zarar ilişkisine neden olmaktadır. Bu sebeple, çalışma

sıcaklıkları ve sürelerinin optimum değerlerini bulma sorunu, reaktörde yüksek enerji verimliliğini sağlamak açısından büyük öneme sahiptir.
Bu tezde, problemin çözümü için birden fazla çözüm yaklaşımı sunulmuştur. Hem parametrik ve istatiksel analiz yöntemi hem de matematiksel optimizasyon metodu yerel optimum çalışma ve sıcaklık değerlerinin bulunması amacıyla benimsenmiştir. Özel reaktör şartları ve alternatif vakalar için farklı yerel optimum değerler hesaplanmıştır.

**Anahtar Kelimeler:** Güneş enerjisi, Hidrojen üretimi, Optimizasyon, Verimlilik

***To my beloved family***

## ACKNOWLEDGEMENTS

Once a wise man said that all that is solid melts into air. So, every thesis has its antithesis resulting in and creating “the change”. Everything flows, and nothing stays same as a fact of universe. In the course of this thesis, I have certainly changed too, for the better or the worse, which can be a topic of another thesis, though I do not know that if anybody would like to read. Readers of this master thesis will not be well versed about the efforts or the long hours spent on writing this thesis or they will never be informed about how I felt or thought while forming every sentence in this study including limited chapters with the intention of being understood. However, since I believe that “It is good to have an end to journey toward; but it is the journey that matters, in the end” as K. Le Guin said, I would like to thank to wonderful people mentioned below that make this journey more colourful and enjoyable with their endless support.

Foremost, I would like to express my deepest gratitude to my advisor Prof. Dr. Deniz Üner for her guidance, encouragement to strive towards better and patience. I wish to thank her not only for her knowledge and enthusiasm but also for being such a motivating, and caring mentor.

I would like to present my sincere appreciation to my co-advisor Assoc. Prof. Dr. Serkan Kıncal for his valuable contribution to my thesis. His great knowledge and kind support have helped me a lot throughout all my thesis.

I also would like to thank my committee members Prof. Dr. Derek K. Baker, Assoc. Prof. Dr. N. Alper Tapan and Assist.Prof.Dr. Harun Koku for their very useful comments and feedbacks.

I wish to thank all members of Uner Group: Deniz Kaya, Mustafa Yasin Aslan, Aziz Doğan İlgün, Necip Berker Üner, especially Atalay Çalışan, and Cihan Ateş for their

excellent support and helpful discussions. I also wish to express my genuine appreciation to Veysi Halvacı and Zeynep Karakaş for their encouragement and kind care. I am also indebted to Taymaz Tabari and Shabnam Jamali for their valuable care and good advises and I am grateful to my colleagues Merve Özkutlu, Berrak Erkmen, Arzu Arslan and Emine Kayahan for their positive attitude, help and friendship.

Special thanks goes to my life-long friend Dilara Yılmaz for her love and endless support. I greatly appreciate my friends Damla Saymazlar, Cansu Yılmaz, İpek Sarı for always being there for me. I am deeply grateful to my dearest friends Mona Shojaei and Navid Mohammadvand for their care, great help and understanding. I also want to express my sincerest gratitude to Şefika Atay for not only being such a caring and supportive friend but also for all the joyful moments and conversations that we had. I want to thank especially Deniz Sun for her great help during the writing part of the thesis, her inspiring talks during the most difficult times and her valuable friendship. I also want to thank my uncle Musa Yavuzyılmaz and Sultan Tekinaslan for being wonderful listeners and advisors during the long and dark time of the soul. I am so thankful to Seda Sivri for being the best roommate ever. I am helpless to acknowledge her spiritual contribution to my life since words are not enough to appreciate her help, support and friendship throughout the last three years.

I would like to express my most sincere gratitude to my brother Onur Yavuzyılmaz and his wife Burcu Şayin Yavuzyılmaz. I appreciate their generosity, patience and motivational talks during the writing of the thesis. I also want to thank my brother for being the greatest brother in the world for me for the last 26 years.

Finally, I would like to express my deepest love and thanks to the people who have made me who I am today, my mother Ülkü Yavuzyılmaz and my father Mehmet Nuri Yavuzyılmaz. It would be impossible for me to finish this journey without their unconditional love and support. In this life, their love is the only and the greatest thing that keeps me going. So, I want to thank them in the simplest, oldest but the most powerful way by just saying I love you with all my heart.

## TABLE OF CONTENTS

## LIST OF TABLES

### TABLES

## LIST OF FIGURES

### FIGURES

## LIST OF SYMBOLS

### SYMBOLS

| | |
|---|---|
| $A$ | Surface area where adsorption takes place |
| $A_r$ | Effective surface area where the heat loss occurs |
| $c_1$ | Water concentration in the feed |
| $c_{p_{CeO_2(s)}}$ | Specific heat of the Redox Material |
| $Ea_{red}$ | Activation energy of reduction step |
| $Ea_{wsp}$ | Activation energy of water splitting step |
| $E_{inert}$ | Energy required to separate the inert sweep gas from air |
| $F$ | Molar flow rate |
| $h$ | Convective heat transfer coefficient |
| $HR$ | Heat recuperation fraction |
| $\Delta H_{red}$ | Enthalpy of the reduction process |
| $\Delta H_{fuel}$ | Higher heating value of the fuel, |
| $k_{c,red}$ | Rate constant for reduction step |
| $k_{c,wsp}$ | Rate constant for oxidation step |
| $k_{red}$ | Reduction rate constant |
| $K_{eq}$ | Equilibrium constant |
| $\dot{n}_i$ | Molar rate of of compound $i$ |
| $N_v$ | Number of vacant sites |
| $N_T$ | Maximum capacity of surface for adsorption |
| $P_i$ | Partial pressure of compound $i$ |
| $Q_{rxn}$ | Total energy consumed by the reduction process |
| $Q_{TC}$ | Net thermal input for the system |

| | |
|---|---|
| $\dot{Q}_A$ | Solar power input at a reactor aperture |
| $\dot{Q}_{ceria}$ | Rate of sensible heat given to the redox material |
| $\dot{Q}_{chem,red}$ | Rate of total energy consumed by the reduction process |
| $\dot{Q}_{con}$ | Rate of energy loss due to convective heat transfer |
| $\dot{Q}_{cool,ox}$ | Excess heat to cool the oxidation side of the reactor |
| $\dot{Q}_{con(red)}$ | Rate of energy loss due to convective heat transfer at reduction step |
| $\dot{Q}_{con(ox)}$ | Rate of energy loss due to convective heat transfer at oxidation step |
| $\dot{Q}_{gases,ox}$ | Energy requirement of the oxidizer gas fed to system |
| $\dot{Q}_{Loss(ox)}$ | Rate of energy loss by convection and radiation at the oxidation step |
| $\dot{Q}_{Loss(red)}$ | Rate of energy loss by convection and radiation at the reduction step |
| $\dot{Q}_{rad}$ | Rate of energy loss due to radiative heat transfer |
| $\dot{Q}_{rad(red)}$ | Rate of energy loss due to radiative heat transfer at reduction step |
| $\dot{Q}_{rad(ox)}$ | Rate of energy loss due to radiative heat transfer at oxidation step |
| $\dot{Q}_{Reaction,red}$ | Rate of total energy consumed by the reduction process |
| $\dot{Q}_{reheat}$ | Rate of sensible heat given to the redox material |
| $\dot{Q}_{rerad}$ | Rate of sensible heat given to the redox material |
| $\dot{Q}_{solar}$ | Rate of energy coming from sun |

| | |
|---|---|
| $\dot{Q}_{sun}$ | Rate of energy coming from sun |
| $\dot{Q}_{water}$ | Sensible and latent heat consumed by the water |
| $r_{desorption}$ | Desorption rate of oxygen |
| $R$ | Gas Constant |
| $t$ | Time |
| $T$ | Temperature |
| $T_a$ | Ambient Air Temperature |
| $W$ | Hydrogen compression work |
| $y$ | Fraction of the surface coverage |
| $T_C$ | Oxidation temperature |
| $T_H$ | Reduction temperature |
| $\eta_{solar-to-fuel}$ | Thermal efficiency for solar to fuel conversion |
| $\eta_{he}$ | Thermal efficiency of heat exchanger |
| $\eta_{overall}$ | Overall thermal efficiency |
| $\eta_{optical}$ | Thermal efficiency of optical system |
| $\eta_{receiver}$ | Thermal efficiency of the receiver |

*Greek Symbols*

| | |
|---|---|
| $\alpha$ | Weight |
| $\varepsilon_s$ | Heat recuperation by solid system |
| $\sigma$ | Stefan Boltzman constant |
| $\eta$ | Thermal efficiency |
| $\delta$ | Nonstoichiometric ratio |
| $\tau$ | Time |
| $\varphi$ | Maximum(allowable) storage capacity of the wall |
| $\Psi$ | Total site number in monolith surface |

*Abbreviations*

| | |
|---|---|
| $GRG$ | Generalized reduced gradient |
| $GAMS$ | General algebraic modeling system |
| $HHV$ | Higher heating value |
| $MO$ | Metal oxide redox material |
| $N/A$ | Not applicable |
| $NLP$ | Nonlinear programming |
| $ROCA$ | Rotating cavity solar reactor |
| $RPC$ | Reticulated porous ceramic |
| $SQP$ | Successive quadratic programming |

# CHAPTER 1

# INTRODUCTION

Hydrogen or “Inflammable air”, the name given by Lord Henry Cavendish in 1766 on the paper “Three papers, containing Experiments on factitious Air” in the journal Philosophical Transactions [1], is one of the most valuable elements. It is the most plentiful element in the universe. Due to its highly reactive nature, it is in the structure of many compounds, such as water and organic compounds. In addition to its abundance in nature, $H_2$ has the highest calorific value compared to other fuels [2]. Also, it can easily be transformed to other energy forms. It can be stored in various forms and as result of that it can be transferred easily to long distances [3]. Therefore, such physical and chemical properties make hydrogen attractive for a diverse range of applications. Hydrogen is consumed in many areas with different purposes such as feedstock in several industries like petroleum refining, ammonia production, or as clean energy carrier. The hydrogen demand of different fields is demonstrated in Figure 1:1. Nowadays, the yearly value of hydrogen market is nearly $420-500 billion and it is expanding with a 20% yearly growth rate [4].

As shown in Figure 1:1, the major part of the hydrogen produced- nearly 96%- is used as chemical reactant in different sectors such as refining, ammonia production, methanol production, saturation with hydrogen in food processing, and metallurgy area.

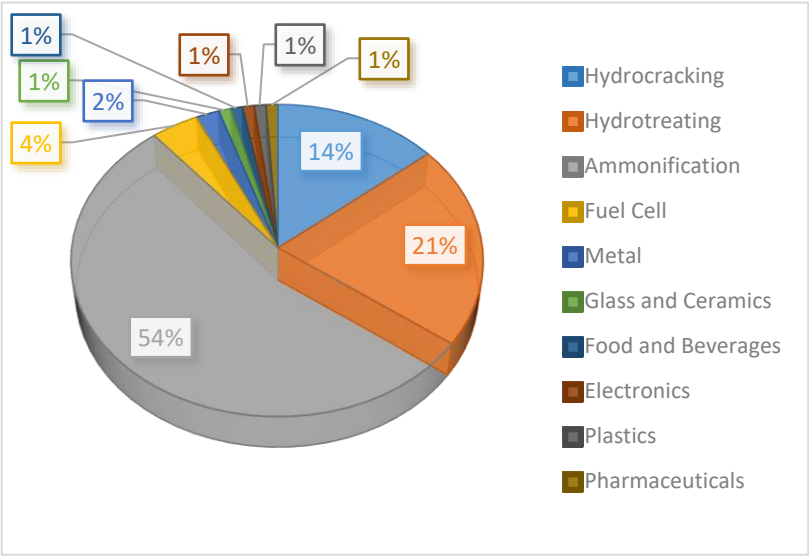


**Figure 1:1** Percentages of hydrogen demand of different fields (Modified from data in [4])

## 1.1 Role of Hydrogen as Energy Carrier

Nowadays, world energy demand increases with the increasing world population which results in various new contemporary problems related to energy production, usage and consumption. Hydrogen can be used as energy carrier like electricity due to its aforementioned properties, i.e. high calorific value, ease in storage and transportation etc. As demonstrated in Figure 1:1, today, only 4% of total hydrogen produced is consumed as energy carrier in fuel cell technology. However, the role of hydrogen as a clean, renewable primary energy source in the energy market is expected to increase. For example, it is predicted that hydrogen will be significant in transportation sector as energy carrier with the aim of reducing the role of carbon based fuels that attributes to the approximately 18% of consumption of world primary energy supplies [5]. In total, annual total hydrogen demand is expected to increase by 5-7% till the year 2018 [4].

## 1.2 Hydrogen production methods

Today, the yearly hydrogen production has reached to values of nearly 50 million metric tonnes [4].

**Table 1:1** Current hydrogen production technologies and their hydrogen supply share (Modified from [4] and [3])

| Feedstock | Energy Source | Production Method | (%) |
|---|---|---|---|
| Natural Gas | Thermal | Steam Methane Reforming | 46 |
| Coal | Thermal | Coal Gasification | 19 |
| Naphtha | Thermal | Oil Reforming | 30 |
| Water | Electrical | Water Electrolysis | 4 |

**Table 1:2** Global warming potential (GWP) of different hydrogen production methods[6]

| Method | GWP (g eq. $CO_2$) |
|---|---|
| Steam Reforming | 9 |
| Coal Gasification | 12 |
| Electrolysis | 8 |
| PV Electrolysis | 3 |
| Photocatalysis | <1 |
| Photoelectrochemical Method | <1 |
| Photoelectrolysis | 2 |

As it can be seen in Table 1:1, a major part -approximately 96%- of hydrogen is supplied by petroleum refining using fossil fuels as both primary energy resource and feedstock, that results in the nearly $107 billion the yearly cost of hydrogen production in 2015 [4]. However, long-term energy security due to scarcity of fossil fuels, air pollution and climate change as a result of green-house gases are important problems for both conventional hydrogen production methods and energy utilization. 85% of particulates and all of SOx and NOx emissions result from energy sector due to fossil fuels, that is the only major contributor of air pollution, the fourth largest danger to human health resulting in nearly 6.5 million deaths each year [7]. Moreover, according to the International Energy Agency, two-thirds of greenhouse gas emissions result from again energy sector based on fossil fuels. Global warming potential of several hydrogen production methods in terms of equivalent gram of $CO_2$ is shown in Table 1:2. More environmental friendly methods for hydrogen production are needed to achieve an average increase below 2℃ with respect to pre-industrial levels; this value was set as a limitation to global warming by governments in the 21st Conference of the Parties of the UNFCCC in 2015 [8]. Therefore, the answer to the problems related to using fossil fuels as primary energy supplies lies in developing new methods based on renewables as primary energy sources to produce hydrogen.

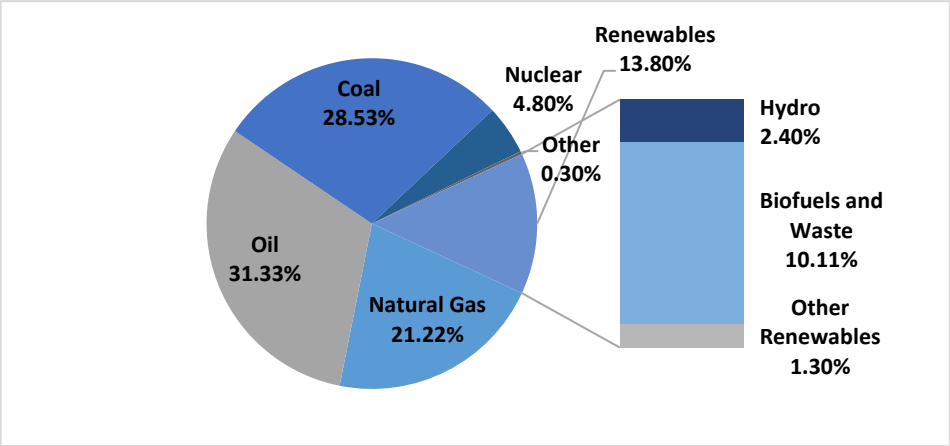


**Figure 1:2** Total primary energy supplies shares for 2014 [9]

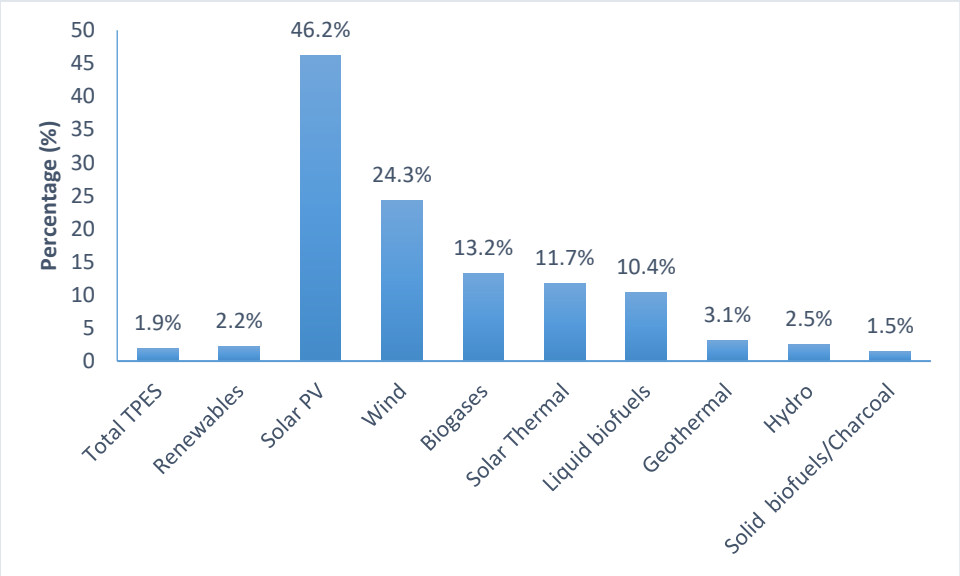


**Figure 1:3** Growth rates of renewable energy sources between 1994-2014 [9]

Today, only 13.80% of total energy supply is produced using renewable energy sources as shown Figure 1:2. However, when the growth rates of renewable energy sources between 1990 and 2014 demonstrated in Figure 1:3 are investigated, it is seen that the increase in renewables are more than the total increase in total primary energy supplies and also the growth rate of solar energy based technologies are higher in comparison to other renewable based methods. It is predicted that renewable energy sources will be dominant in electricity generation in 2050 [5].

## 1.3 Solar Hydrogen Production Ways

Nowadays, solar energy constitutes nearly 2.5% of the total renewable energy supply as illustrated in Figure 1:4. Sun is a huge renewable source of power. Every day the amount of power supplied by the sun for to Earth is approximately $1.7\times10^5$ TW (Vayssieres, 2010). However, solar power has a periodic behaviour, in other words, the power of sun is only available in day-time. Thus, it is difficult to use this power in night-time without storing. Solar hydrogen production is way of storing solar energy in chemical bonds in order to use this energy when it is needed.

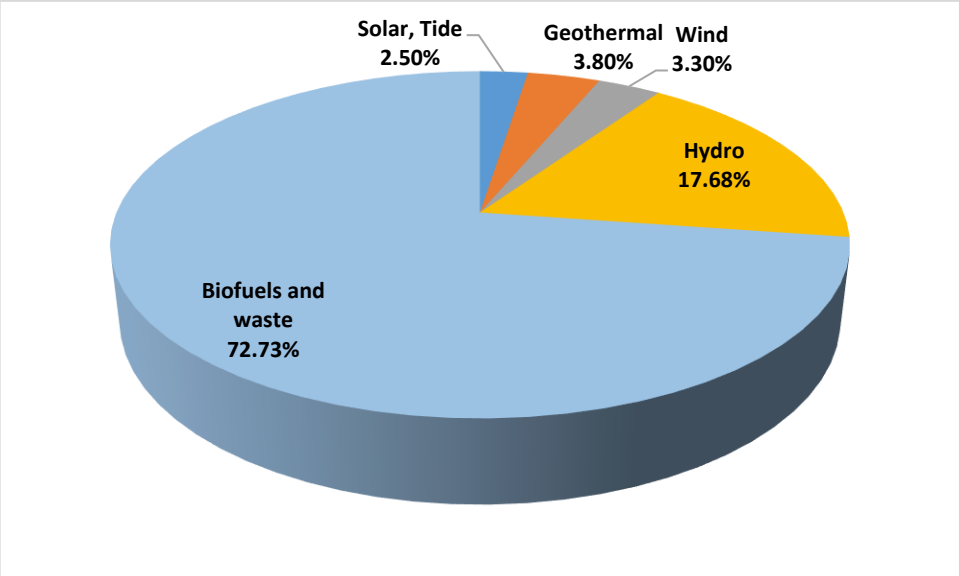


**Figure 1:4** Contributions of renewable energy sources to world energy [9]

Solar hydrogen can be produced using electrochemical, photochemical, photobiological and thermochemical methods. Thermochemical methods use concentrated solar radiation to produce hydrogen from raw material by the realization of endothermic chemical conversion at high temperatures [11].

**Table 1:3** Hydrogen production methods using concentrated sun power. Tabulated by using ref. [11]

| Method Name | Raw material |
|---|---|
| Direct Thermolysis | Water |
| Solar Thermochemical Cycles | Water |
| Solar Reforming | Water, Fossil Fuel |
| Solar Cracking | Fossil Fuel |
| Solar Gasification | Water, Fossil Fuel |

As can be understood from Table 1:3, only water as raw material is consumed by two of the methods, direct thermolysis and solar thermochemical cycles, while fossil fuel is required for the rest of the three methods. Therefore, it can be concluded that direct thermolysis and solar thermochemical cycle methods are advantageous when their environmental impact is considered. In other words, they are more eco-friendly in comparison to their competitors since there is no need for fossil fuel in these methods. In thermolysis, water splits into its components in a single endothermic reaction. However, in the thermochemical cycle method, water dissociation occurs in two or more steps by means of an intermediate substance. Although both thermolysis and thermochemical cycle methods are environmentally friendly ways of producing hydrogen from water, the solar thermochemical cycle method is more advantageous since direct thermolysis requires excessive high temperatures and spontaneous product separation to drive the single step reaction [12].

**Table 1:4** Reaction steps and temperatures for copper-chlorine thermochemical cycle[13]

| **Reaction Steps** | **Temperature (ºC)** |
|---|---|
| $2CuCl_2(s) + H_2O(g) \longrightarrow Cu_2OCl_2(s) + 2HCl$ | 450 |
| $Cu_2OCl_2(s) \longrightarrow 2CuCl(l) + 1/2O_2(g)$ | 500 |
| $4CuCl(aq) \longrightarrow 2CuCl_2(aq) + 2Cu(s)$ | 25 |
| $2CuCl_2(aq) \longrightarrow 2CuCl_2(s)$ | 90 |
| $2Cu(s) + 2HCl(g) \longrightarrow 2CuCl(l) + H_2(g)$ | 450 |

In the literature, there are numerous thermochemical cycles for the solar hydrogen production [14]. One of the first utilization of this technology is based on supplying the energy requirement of thermochemical cycles by waste heat from nuclear energy,

while thermochemical cycles with more than two steps with average temperatures are used to produce hydrogen with corrosive intermediate substances. One of the examples of this kind of thermochemical cycles, the copper-chlorine cycle is shown in Table 1:4. There are many other commercial cycles using corrosive materials such as sulphur-iodine (Se-I), cerium-chlorine (Cu-Cl), Cerium-Chlorine (Ce-Cl), Iron-Chlorine (Fe-Cl) etc.[13].

A two-step thermochemical cycle using metal oxides instead of corrosive materials as reducing agent shown below was first offered by Nakamura [15]. Nowadays, there are numerous two-step thermochemical cycles in the literature using various redox materials to produce hydrogen from water.

## 1.4 Energy Efficiency and Cost Issues

Table 1:5 shows the energy efficiencies and unit hydrogen production costs for both conventional and newly developed alternative renewable hydrogen production ways.

**Table 1:5** Energy efficiencies and unit hydrogen production costs for different hydrogen production methods( [6] - [16])

| Hydrogen Production Method | Energy Efficiency | Average Unit Hydrogen Production Costs ($/kg Hydrogen Produced) |
|---|---|---|
| Fossil Fuel Steam Reforming | 60-80 | ~0.8 |
| Coal Gasification | 40-60 | ~1 |
| Electrolysis | ~50 | ~2.8 |
| Solar PV | 19.8 | N/A[1] |
| Solar Photoelectrochemical | 12.4 | N/A[1] |
| Photobiological | < 10 | N/A[1] |
| Concentrated Solar Energy via Thermal Cycling | ~15 | N/A[1] |

[1]Lab scale information could not be translated into industrial scale economics.

**Table 1:6** Predicted hydrogen production costs for solar technologies

| Hydrogen Production Method | Predicted Average Unit Cost for Hydrogen Production ($/kg Hydrogen Produced) | Prediction Year |
|---|---|---|
| Solar PV Electrolysis | 6.7-10.7 | 2020[a] |
| Solar Photoelectrochemical | 3.5 | 2014[b] |
| Concentrated Solar Energy via Thermal Cycling | 3.9-5 | 2020[a] |

[a][17]

[b][16]

As can be understood from Table 1:5 and Table 1:6, the most important obstacles for the commercialization of solar thermochemical hydrogen production via water splitting are the high production costs and low energy efficiencies. Therefore, the competitiveness of solar thermochemical hydrogen production in the market strongly depend on increasing energy efficiency, the main idea of this study.

# CHAPTER 2

# LITERATURE REVIEW

## 2.1 Background Information

In this section, brief background knowledge related to solar thermochemical hydrogen production from water via metal oxides is presented in order to provide an underlying idea to grasp the concepts of energy efficiency and monolith reactors. Information explained in literature studies given in Section 2.2 form a basis for this thesis.

### 2.1.1 Solar Thermochemical Water Splitting Systems

As mentioned in previous sections, there have been many proposed cycles for solar thermochemical hydrogen production consisting of two or more steps in the literature. However, two-step thermochemical cycles using metal oxide as redox material are the most favourable ones since they have higher efficiencies compared to other cycles [11].

Many researches have been performed with numerous metal oxides as redox materials showing thermal and overall efficiencies of the system. The conceptual general reaction steps are shown by Chueh and Haile [18] as follows;

$$\frac{1}{\delta} MO_y \rightarrow \frac{1}{\delta} MO_{y-\delta} + \frac{1}{2}\, O_{2\,(g)} \qquad \text{Step 1}$$

$$H_2O_{(g)} + \frac{1}{\delta} MO_{y-\delta} \rightarrow \frac{1}{\delta} MO_y + H_{2\,(g)} \qquad \text{Step 2}$$

In this reaction scheme, MO represents a metal oxide redox material and $\delta$ symbolizes the nonstoichiometric ratio.

The aforementioned two-step thermochemical solar hydrogen production technology from water using metal oxides as redox material was first suggested by Nakamura [15]. In that paper, while the mechanism for two-step thermochemical cycle of iron oxide redox pair ($Fe_3O_4$/FeO) is introduced to the solar-thermal literature, the thermal efficiency of this two-step cycle is also investigated:

$$Fe_3O_4 \rightarrow 3FeO + \frac{1}{2}\, O_2 \qquad \text{Step 1}$$

$$H_2O + 3\, FeO \;\rightarrow\; Fe_3O_4 + H_2 \qquad \text{Step 2}$$

In step 1, the endothermic reaction driven by solar energy takes place. In other words, the metal oxide redox material is reduced at high temperature and oxygen in the structure of metal oxide is released to the environment during the decomposition process. In the next step, step 2, reduced metal oxide is oxidized by water vapour at low temperatures as oxygen in the structure of water is captured by reduced metal oxide by splitting it into hydrogen and oxygen. At the end of oxidation process occurring in step 2, hydrogen is obtained and the thermochemical cycle is completed by returning metal oxide to its initial condition.

Process flow scheme of solar thermochemical hydrogen production from water can be generalized as shown in Figure 2:1. In the process flow scheme, sunlight first encounters the solar concentrating system. Solar concentrating system consists of heliostat fields and a concentrator, that is responsible for collecting and projecting sunlight coming from the sun to the focal point on the solar thermochemical reactor. In solar thermochemical reactor, two-step thermochemical reaction of redox material takes place after exposing the concentrated solar energy coming from concentrator. Aforesaid, in the thermochemical cycle, first thermal decomposition of the redox material occurs at high temperature due to the concentrated solar energy as driving

factor. Then, the reactor is cooled to average temperature levels and water is supplied to the reactor: As a result of that, redox material is oxidized while produced hydrogen is swept by inert gas or by vacuum pump. If sweep gas is used, an additional separation unit is necessary to differentiate gas product stream to obtain hydrogen in a pure form.

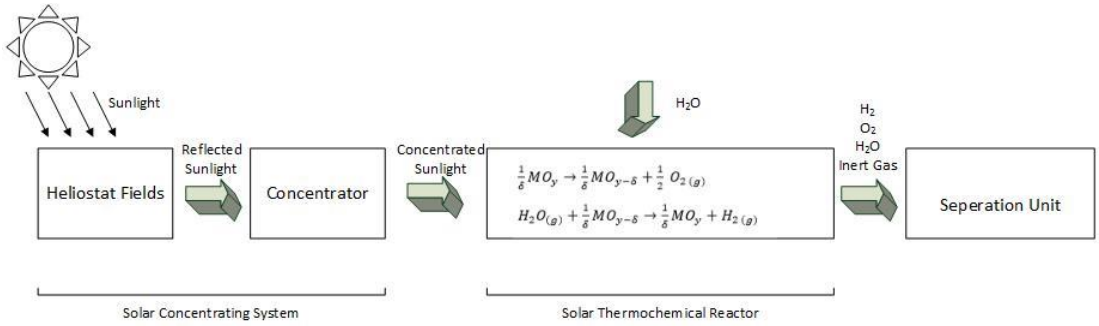


**Figure 2:1** The general process flow diagram of solar two-step thermochemical hydrogen production via metal oxide

### 2.1.2 Modeling Monolith Reactors

It is obvious that the heart of the solar thermochemical hydrogen production technology is the reactor unit wherein all the thermochemical cycle is completed. Many novel reactor types have been suggested in the literature as well as conventional ones. Since thermochemical cycle can be regarded as a gas-solid multiphase system, conventional reactors such as fixed bed or packed bed is suitable to carry out the thermochemical cycle [19]. In addition to conventional reactor types for catalytic systems, many novel reactor types such as rotating cavity solar reactor (ROCA), two-cavity solar reactor, ZIRRUS reactor, cavity receiver porous monolithic ceria or dual porosity reticulated porous ceramic (RPC) foam have also been proposed by various studies in the literature [20]. In the following part, brief background information

related to monolithic reactors is presented, since monolithic reactor heat and mass transfer models are used in this study.

Monolith reactors are made up of arranged catalyst structures and have several different structures such as honeycomb and foam [21]. Since they act as catalyst support, they can be used in a wide range of application areas, mostly in automobile industry as catalytic converter to decrease pollutant amount in waste gases [22]-[23]. They can be modelled at different scales for single channel or multiple channel conditions ([21][24]). Single channel modeling seems the most suitable scale to achieve reactor optimization, to evaluate performance of the reactor and to obtain concentration and temperature profiles [21].

Monolithic reactors are advantageous for solar thermochemical hydrogen production via redox material technology, since they allow the reaction to be performed in a single unit and prevent hydrogen from combining with oxygen again [23]. Moreover, lower operation temperatures can be obtained with monolithic reactors in comparison to other cycles [23]. Therefore, there are many studies in the literature to model monolith reactors for solar thermochemical hydrogen production via redox material in a realistic way.

A multi-channelled honeycomb reactor model was presented by Agrafiotis *et al.* for the solar thermochemical hydrogen production system [25] in 2005 as part of HYDROSOL project. In later years in the scope of same project, Dersch *et al.* introduced a two dimensional dynamic model of single-chamber monolith reactor by simulating on Modelica [26]. Again, Agrafiotis *et al.* [27] worked on the design parameters of monolithic reactor for solar hydrogen production technology by presenting a one-dimensional model for heat and mass transfer equations in the single channel in 2007. They used first order reaction rates for production of hydrogen and oxygen adsorption in mass conservation equations in the model. In 2009, a more general model for heat and mass transfer dynamics and reactions kinetics was suggested by Petrasch *et al.* [28]. However, one of the most comprehensive studies about honeycomb monolith reactor models at different levels was introduced to

literature by Kostoglou *et al*. [29]. In this study, they modelled honeycomb at three different scales. As the result of the study, it was concluded that one-dimensional level was suitable for honeycomb monoliths.

In 2015, Furler and Steinfeld [30] presented a 3-D transient mathematical model for cavity receiver reticulated porous ceramic foam solar reactor to analyse topics such as geometrical design, alternative flow structures, temperature distribution etc. Both governing equations for heat and mass transfer are shown in the study for monolith reactor.

Lange *et al.* [31] constructed a three-dimensional dynamic model of monolith reactor for thermochemical water splitting process. In the study, a mathematical model composed of mass, energy and momentum conservation equation for one-dimensional was presented and analysed at different working conditions. Yuan *et al.* [32] also presented a mathematical model for solar monolith reactor for liquid metal oxides to assess the efficiency of the reactor in terms of many performance criteria in a thermodynamic point of view.

### 2.1.3 Efficiency of the System

Efficiency of system is a general term that can be defined based on the expected performance criteria. In this context, efficiency concept can be evaluated in terms of various aspects for a solar thermochemical hydrogen production process. For example, hydrogen yield or the total energy loss during the complete cycle can be efficiency indicator for this system. However, efficiency of the process is generally evaluated in terms of thermodynamic approach, due to the fact that the process path is a thermochemical cycle just like any other thermodynamic cycle. Thus, in the literature most of the works set Carnot cycle efficiency as limiting upper bound [33]. Both exergy efficiencies -second law efficiencies- and solar -to-fuel efficiencies -first law efficiencies- can be calculated theoretically in thermodynamic analysis for each component individually in process flow diagram in Figure 2:1. Exergy is a thermodynamic term that is used to define the maximum work that can be obtained

by the system and its environment [34]. Thus, exergy efficiency is defined as the electricity equivalent of work obtained by the system divided by total input exergy, while the thermal energy is defined as energy output of the system divided by energy input of the system [35].

There are many different definitions in the literature for thermal efficiency since different parameters are taken into account in each one. Table 2:1 shows some of the thermal efficiency definitions of selected works for solar fuel conversion.

**Table 2:1** Thermal efficiency definitions of selected works for solar to fuel conversion

| Reference | Redox Material | Thermal Efficiency Definitions | $Q_{solar}$ Definition |
|---|---|---|---|
| Chueh and Haile [18] | Cerium Oxide | $\eta_{solar-to-fuel} = \frac{285.8\ kJ}{Q_{solar}}$ | N/A |
| Chueh et al. [36] | Cerium Oxide | $\eta_{solar-to-fuel} = \frac{n_{fuel} \times \Delta H_{fuel}}{P_{solar} + n_{inert} \times E_{inert}}$ | N/A |
| Nakamura[15] | Ferrite Oxide | $\eta_{HHV} = \frac{-\Delta H_f}{Q_{heat} + \frac{W}{\eta_{he}}}$ | N/A |
| Diver et al. [37] | Ferrite Oxide | $\eta_{solar-to-fuel} = \frac{n_{H_2} \times HHV}{Q_{solar} + \frac{W}{0.4}}$ | N/A |
| Charvin et al. [38] | Ferrite Oxide and Zinc Oxide | $\eta_{overall} = \eta_{optical}\eta_{receiver}\frac{F_{H_2} \times HHV_{H_2}}{Q_{chemical}}$ | N/A |
| Scheffe and Steinfeld [39] | Cerium Oxide | $\eta_{solar-to-fuel} = \frac{n_{H_2} \times HHV}{Q_{solar}}$ | $Q_{solar} = \left\{\left[\Delta H_2O_{298K \to T_L} n_{(H_2O),} + \int_{T_C}^{T_H} C_{p,CeO_2} dT\right] \times (1 - HR) + \Delta H_{red}\delta\right\} / n_{absorption}$ |
| Venstrom et al. [40] | Cerium Oxide | $\eta_{solar-to-fuel} = \frac{n_{H_2} \times HHV}{Q_{solar}}$ | N/A |
| Lapp et al. [41] | Nonstoichiometric Cerium Oxide | $\eta_{solar-to-fuel} = \frac{\dot{n}_{H_2} \times HHV}{\dot{Q}_{solar}}$ | $\dot{Q}_{solar} = \dot{Q}_{rerad} + \dot{Q}_{CeO_2} + \dot{Q}_{ox} + \dot{Q}_{other} + \dot{n}_{N_2}\left[\bar{h}_{N_2}(T_2) - \bar{h}_{N_2}(T_0)\right] + \dot{n}_{O_2}\bar{h}_{O_2}(T_2) + \dot{n}_{H_2}\bar{h}_{H_2}(T_4) - \dot{n}_{H_2O}\bar{h}_{H_2O(l)}(T_0)$ |

**Table 2:2** (cont'd)

| Reference | Redox Material | Thermal Efficiency Definitions | $Q_{solar}$ Definition |
|---|---|---|---|
| Siegel et al. [42] | Cerium Oxide | $\eta_{con} = \frac{\Delta H_{fuel}}{Q_{TC}}$ | $Q_{TC} = Q_{rxn} + Q_{reheat} + Q_{pump\ work}$ |
| Bader et al. [43] | Cerium Oxide | $\eta = \frac{\dot{n}_{H_2} \times \mathrm{HHV}_{H_2}}{\dot{Q}_{solar}}$ | $\dot{Q}_{solar} = \dot{Q}_{rerad} + \dot{Q}_{heat\ loss} - \dot{Q}_{chem,red} + \dot{Q}_{gases,red} - \dot{Q}_{chem,ox} + \dot{Q}_{gases,ox} + \dot{Q}_{cool,ox} + \dot{Q}_{ceria}$ |
| Ermanoski et al. [44] | Cerium Oxide | $\eta_{TC} = \frac{\dot{n}_{H_2} \times HHV_{H_2}}{P_{TH}}$ | N/A |
| Ermanoski et al. [45] | Cerium Oxide | $\eta_{TC} = \frac{\dot{n}_{H_2} \times HHV_{H_2}}{\dot{Q}_A}$ | N/A |
| Ermanoski [46] | Cerium Oxide | $\eta_R = \frac{\dot{n}_{H_2} \times HHV_{H_2}}{\dot{Q}_A}$ | N/A |
| Lange et al. [33] | Cerium Oxide | $\eta = \frac{W_{use}}{Q_{in}}$ | N/A |
| Yuan et al. [32][a] | | $\eta_{solar\ to\ chemical} = \frac{\dot{n}_{H_2} \times HHV}{Q_{total}}$ | $Q_{total} = Q_{reheat} + Q_{loss} + Q_{RXN} + Q_{purge} + W_{pump}$ |

[a] For the redox material part.

The efficiency of a two-step thermochemical cycle can be increased by enhancing redox material properties or designing reactors with better reactor properties or finding optimum working conditions. For redox material properties, there are a great deal of literature works related to process efficiency based on lab-scale experiments to enhance the metal oxide properties such as stability, oxygen capture capacity, reaction kinetics etc. considering micro-to-macro relations in each cycle [47]. Selecting the suitable reactor design is also one of the biggest challenges encountered by solar thermochemical systems in pilot scale [48]. Reactor properties such as surface area, and heat recuperation can significantly affect the efficiency of the cycle. For example, for many cases, energy efficiency increases as the solid phase heat recuperation increases.

**Table 2:2** Operation temperatures for different redox materials (modified from [49] and [50])

| Reference | Thermochemical Cycle | Reduction Temperature (K) | Oxidation Temperature (K) |
|---|---|---|---|
| [15] | $Fe_3O_4$ / FeO | 2500 | <1000 |
| [51] | $Mn_3O_4$ / MnO | 1810 | 900 |
| [51] | $Co_3O_4$ / CoO | 1175 | 900 |
| [51] | $Nb_2O_5$ / $NbO_2$ | 3600 | 900 |
| [52] | Zn / ZnO | 2273 | 1446 |
| [50] | $In_2O_3$ / $In_2O$ | 2473 | 1073 |
| [50] | $SnO_2$ / SnO | 2973 | 873 |
| [50] | Mo / $MoO_2$ | 3986 | 1816 |
| [50] | W / $WO_3$ | 4183 | 1157 |

Working conditions also have major significance to improve the energy efficiency of the reactor. Moreover, for an established environment and system, it is easier to change operation conditions to enhance the efficiency of the system. In solar thermochemical hydrogen production system via redox material, oxidation and reduction temperatures and pressures are the most important variables that can alter the hydrogen yield and as result of that, efficiency of the cycle. Operation temperatures can change in a range since thermodynamic nature of the redox material sets an allowable range for the working temperatures. Therefore, to obtain maximum efficiency, it is important to find optimum temperature values in that allowable range. Some of the temperatures for different redox materials worked in literature are tabulated in Table 2:2.

## 2.2 Literature Review

### 2.2.1 Energy Efficiency of Solar Thermochemical Water Splitting Systems

Due to aforementioned reasons, it is very crucial to increase energy efficiency while decreasing the cost factor for solar thermochemical hydrogen production technology from water via redox material in terms of the economic sustainability of the method. Therefore, in recent years an increased interest has been observed in this area, the field of optimal design and working conditions of solar thermochemical systems to make this technology compete with its opponents in hydrogen production market. Reducing the cost items and enhancing the efficiency of the production by improving either energy gain or hydrogen yield are the two main courses of action that have been the main subjects of several studies and both of the two actions have been conducted at several different scales from micro-scale to macro-scale theoretically and also from lab-sized to demonstration-sized scale experimentally.

Overall, solar-to-hydrogen conversion efficiency of the solar thermochemical hydrogen production process scheme is affected by the efficiencies of each unit demonstrated in Figure 2:1 in Section 2.1.1. For solar concentrating system, energy efficiency is defined as the ratio of conversion solar energy to chemical energy by

Steinfeld [11] and in literature several studies exist to increase energy efficiency of this system. Details of some of the mentioned works are given in Table 2:3.

**Table 2:3** Selected literature work examples on optimization of solar concentrating systems

| Reference | Optimization Unit | Decision Variable | Method |
|---|---|---|---|
| [53] | Concentrator | Operating temperatures | Simulation |
| [54] | Receiver | Flux density Distribution/Proper Distribution of Heliostats | TABU Algorithm/Metaheuristics |
| [55] | Heliostat Field | Selection of Heliostats in order to control temperature | Combinatorial Algorithm to solve Knapsack Problem |

However, although technology of solar concentrating systems are quite developed and there is no room for improvement which results in a significant change on overall efficiency as stated by Siegel *et al*. [42], it is also important to address the efficiency of solar thermochemical systems in terms of optimized kinetic and transport processes.

### 2.2.2 Thermochemical Reactor Efficiency

The process of conversion of solar energy to chemical bond energy by producing hydrogen via two-step thermochemical cycle of any metal oxides in a solar thermochemical reactor has some challenges due to nature of the process causing thermochemical limitations and energy losses. In order to find solution to these

challenges, numerous studies, both theoretical and experimental are present in the literature associated to efficiency of two-step thermochemical cycle.

A thermal analysis based on the a newly proposed thermochemical cycle of manganese oxide as redox material and sodium hydroxide as hydrogen source was conducted by Sturzenegger and Nüesch [56] to improve the working temperatures. While neglecting re-radiation losses, overall thermal energy loss is calculated as 74% at overall. The study also shows that huge increase in re-radiation losses occurs with increasing reduction temperatures. As the result of the experimental analysis, Chueh and Haile [18] prove that reduction temperature as an important factor that affects the efficiency of the cycle.

Chueh *et al.* [36] show that energy losses due to radiative and conductive heat transfer affects energy efficiency significantly as the conclusion of the experimental data of cerium oxide thermochemical cycle. Moreover, they conclude that reactor design and scaling parameters are more important in terms of solar-to-fuel efficiency compared to redox material properties.

Lapp *et al.* [41] conducted a parametric thermodynamic study for dual-zone isobaric solar thermochemical reactor with two heat exchanger at the exit and entrance of the reactor wherein nonstoichiometric ceria takes place as redox material. In the study, steady-state energy balances around the reactor were modelled and used in thermal efficiency calculations whose definition tabulated in Table 2.1 in Section 2.1.1. Outcomes of thermal efficiency, fuel production and exergy efficiency were evaluated separately with respect to the changes in working conditions such as reduction step pressures as well as the changes in material properties such as heat recovery of solid and gas phases, nonstoichiometric ratio of ceria. The study concludes that heat recovery from the solid phase potential is an important factor contributing to the thermal efficiency. Also, thermal efficiency increases as the gas phase heat recovery and nonstoichiometric ratio of reduction increase individually. So, it can be said that the amount of the oxidizing material and sweeping gas are also important design parameters in terms of thermal efficiency as a natural consequent.

In the study, it is also pointed that the optimum reduction temperature can be found by using the trade-off between increasing heat losses due to re-radiation and decreasing heat loss due to improper heat recovery of solid phase as reduction temperature increases.

A theoretical thermodynamic study to show the factors affecting thermal efficiency of solar thermochemical system was carried out by Siegel *et al.*[42] for a specified thermochemical heat engine to produce fuel (CO). In this specified thermochemical heat engine system, a fuel cell converts produced fuel to work in addition to thermochemical cycle. So, Siegel *et al*. [42] made a parametric thermodynamic analysis based on the thermal efficiency shown in Table 2.1. However, their thermal efficiency definition only included the energy requirement of the endothermic reduction reaction, energy to reheat the metal oxide material from oxidation temperature to reduction temperature and energy spent on the sustaining oxidation stage pressures. Heat losses due to convection and conduction were neglected and heat losses due to reradiation was included in the collector efficiency but not thermal efficiency calculation. Also, the study excluded the sweep gases in evaluation. For different values of reduction temperature, partial oxygen pressure at reduction step and reaction extent, thermal efficiencies were evaluated between 32-65% theoretically and overall efficiency trends were plotted based on the defined utilization factor. In the study, it is concluded that heat recuperation and reaction extent are two important parameters that affects overall efficiency in a great deal. Also, it is said that although it is advantageous to increase the gap between oxidation and reduction temperatures in thermodynamic point of view, it causes trade-off in terms of requirement of reheating energy of redox material and recuperation costs.

Bader *et al.* [43] also performed a thermodynamic analysis on solar thermochemical fuel production system for ceria redox material. In the study, same dual thermochemical system with Lapp *et al.* [41] was evaluated at isobaric conditions. Effects of several parameters such as operating temperatures, partial oxygen pressure and gas phase heat recovery, purity of sweep gas and temperature change between reduction and oxidation temperatures on thermal efficiency in Table 2:1 were

investigated. According to their results, Bader *et al.* [43] concluded that thermal efficiency increases highly even for slight increases in temperature difference between oxidation and reduction temperatures. Moreover, they pointed out that thermal efficiency increases as gas phase heat recuperation increases and total system pressure decreases. In the study, it is also mentioned that energy spent on heating of sweep gas is major part of energy costs which makes sweep gas flow rate important factor.

In 2013, a new reactor design applying moving particle bed concept to improve cycle efficiency was suggested by Ermanoski *et al.* [44]. The design was evaluated in terms of thermal efficiency by conducting a thermodynamic parametric analysis. The thermal efficiency definition for this study is shown in Table 2:1.

Unlike the parametric thermodynamic studies explained previously, a simulation based thermodynamic analysis for solar-receiver reactor was carried out in an plant model in Aspen by Houaijia *et al.* [57]. In the study, efficiency of thermal cycle was expected to increase by changing the design of the reactor to decrease radiative heat losses. They showed that more than 25% thermal efficiency increase was achieved by changing the design of the reactor for instance cavity design with the aim of less re-radiation losses.

Ermanoski *et al.* [45] performed and analysis determining optimal working temperature for isothermal solar thermochemical cerium oxide cycle. In a thermodynamic view, efficiency is defined shown in Table 2.1 and trendlines for this efficiency definition were obtained by changing oxygen partial pressure at reduction step and temperature difference between oxidation and reduction steps individually. Efficiency decreased as the partial pressure at reduction phase increased. Increasing temperature difference change demonstrated a concave trendline for reactor efficiency. One of the important results of this study was that isothermal reactors were significantly less efficient than the reactors in which temperature change between oxidation and reduction steps occurred so, it is commented that temperature swing and pressure swing reactors are favourable for this method in the future.

In 2014, Lange *et al.* [33] published a paper related to temperature-entropy analysis of the solar thermochemical two-step hydrogen production for several changing parameters. The analysis excluded the re-radiation losses, and gas and solid phase heat recuperation and oxygen partial pressure reduction. In the study, by comparing direct thermolysis, it was said that the second step for thermochemical cycle was necessary in terms of entropy calculation result. Moreover, a parametric study and pinch point analysis for different working temperatures, pressures and water conversion were conducted in the study.

A similar thermochemical cycle to hydrogen production cycle that is carbon monoxide production from carbon dioxide via solar thermochemical way was investigated by Venstrom *et al.*[40]. Although the product is not hydrogen, this study results are taken into consideration since information related to sweep gas factor is presented. According to study, as the sweep gas rate increases, the pressure drop also increases. For sweep gas rate, system was mass transfer limited for small rates and at high flow rates, it was found as surface kinetic limited. Also, gas and solid phase heat recuperation was analysed thermodynamically and same conclusion with hydrogen that was as the recuperation increased, thermal efficiency increased.

In 2014, Ermanoski [58] proposed a change in the design of the single chamber reactor and suggested a new method for low partial oxygen pressure at reduction phase which resulted in increase in efficiency. In conventional methods, vacuum pumping or sweeping gas is used to obtain low oxygen partial pressures. Instead of these methods, Ermanoski offered to use cascaded chambers for reduction step where pressure was gradually lowered. It was concluded that efficiency gain in this method was significant in comparison to efficiency of conventional ways.

Ermanoski [46] in 2015 investigated working conditions and material requirements for two-step solar thermochemical to maximize the efficiency of the cycle. By optimizing working temperatures and lowering partial pressure of the oxygen in reduction step, numerical calculations were done in the study with the aim of obtaining maximum efficiency. Thermochemical efficiency definition considering all

re-radiation heat loss, sensible heating of feed water, mechanical works, endothermic energy requirement of the reaction are shown in Table 2:1. It is concluded that each of the factors, both temperatures and the partial pressure of the oxygen, increase the efficiency of the cycle individually to an important degree.

One of the most detailed comprehensive studies in the area of energy efficiency of water splitting thermochemical cycles was presented by Jarrett *et al.* in 2016 [59]. In this study, the assumptions related to energy efficiency that were not considered in models stated by previous studies were relaxed and it is shown that relaxation of these assumptions such as energy required to preheat the metal oxide create large differences on the working conditions of the reactor. By performing numerical analysis of suggested thermodynamic reactor model to see the effect of these relaxations on the energy efficiency, they proposed new way to compare redox materials with each other in terms of maximum energy efficiency obtained by the system. Also, critical limitations of the analysed parameters are discussed.

The studies mentioned above up-to this point all are only based on thermodynamic model based on steady-state working conditions and does not consider the time dependency of working conditions such as temperature and reduction pressure. based on reaction kinetics or heat and mass transfer mechanism. As can be seen from the thermal efficiencies data tabulated in Table 2:4, the calculated theoretical efficiencies by using thermodynamic models have very high values compared to experimental efficiencies obtained by reactor data in reality like shown in work of Chueh e*t al.* [36]. Keene *et al.* [60] showed that this big difference is due to the transient nature of the both temperature and partial oxygen pressures. So, they concluded that one should certainly consider reaction kinetics, heat and mass transfer mechanism to get closer values of thermal efficiencies. Therefore, studies explained below are important to obtain accurate efficiency values in this area.

Lapp *et al.* [61] worked on transient heat transfer 3-D model of solar counter-rotating cylinder reactor. In the study, 3-D model was built by coupling energy balance equations considering radiative, convective and conductive heat transfer mechanism

and mass balance equations considering only reduction reaction kinetics. Since reaction kinetics were unknown, linear dependency of stoichiometric ratio on time was assumed. According to results of this study, more realistic values like 4.8% thermal efficiency was obtained.

Yuan *et al.* [32] also worked on a simulation of solar thermochemical reactor model to determine thermal efficiency. Different from the other works, Yuan *et al.* offered a novel reactor design based on liquid metal oxide as redox material and as a result of that different thermal efficiency definition. They defined two separate efficiencies that were solar-to-chemical efficiency showing and solar-to thermal efficiency.

Lange *et al.* [31] conducted an efficiency analysis on dynamic model of monolith reactor for solar thermochemical hydrogen production. Mathematical modeling of the monolith reactor was done by stating energy, mass and momentum conservation equations as well as indicating reaction kinetics. By changing maximum oxygen capacity, reaction kinetics and loading of the redox material, optimum conditions for some parameters such as sweep gas flow rate, feed water flow rates were estimated and their influence on efficiency was monitored.

Chandran *et al.* [62] also carried out an analysis based on evaluation of 3-D heat and mass transfer mechanism on a novel reactor on ANSYS. Model was simulated and transient temperature, heat flux oxygen release rate, non-stoichiometry profiles were obtained for the selected time periods. Although the study does not contain work related to obtain maximum thermal efficiency, based on the profiles it is said that lower partial oxygen pressures and higher reduction temperature result in high oxygen release in reduction step. Also, they concluded that reduction step is mass transfer bounded and dependent on surface kinetics based on the selected reaction kinetics rather than heat transfer mechanism.

**Table 2:4** Thermal efficiencies of solar thermochemical hydrogen production for selected literature studies

| Authors | Metal Oxide | Theoretical / Experimental | Operating Temperatures | Thermal Efficiency (%) |
|---|---|---|---|---|
| Chueh et al. [36] | Nonstoichiometric cerium oxide | Experimental | 1913 and 1693 K- 1173 K | 0.7-0.8 |
| Sturzenegger and Nüesch [56] | Manganese oxide as redox material<br>Sodium as hydrogen source | Theoretical | 1835 K – 900 K | 51-42[b]<br>36-26[d] |
| Chueh and Haile [18] | Nonstoichiometric cerium oxide | Theoretical | 1773 and 1873 K -1073 K | 16-19 |
| Steinfeld[52] | ZnO | Experimental | 2300 K- 700 K | 29[a] |
| Lapp et al. [41] | Nonstoichiometric cerium oxide | Theoretical | 1073 K | 4.4-40.8 |
| Nakamura[15] | Ferrite Oxide | Theoretical | 2500 K- <1000 K | 35[b]<br>>60[c] |
| Diver et al. [37] | Ferrite Oxide | Theoretical | N/A | 36[b]<br>76[c] |
| Charvin et al. [38] | Ferrite Oxide | Theoretical | N/A | 10.3-15.6[c] |
| Charvin et al. [38] | Zinc Oxide | Theoretical | N/A | 10.1-18.1[c] |
| Scheffe and Steinfeld [39] | Cerium Oxide | Theoretical | N/A | 20.2[b]<br>29.5[c] |
| Siegel et al.[42] | Cerium Oxide | Theoretical | 1773 K - 373 or 1073 or 1473 K | 32-65 |
| Bader et al. [43] | Cerium Oxide | Theoretical | 1773 K<br>1773 K-1673 K | 10<br>31.6 |
| Ermanoski et al. [44] | Cerium Oxide | Theroretical | 1773 K – 1373 K | >30 |

[a]Exergy efficiency [b]No heat recovery
[c]Heat recovery [d]With air

## 2.3 Motivation of the Study

Today, increasing the efficiency of solar thermochemical reactor for two-step solar thermochemical hydrogen production method constitutes the major part of the efforts spent on the development of this renewable technology and it is one of the main concerns for the viability of this technology. So, since 2012, there is a growth in the number of studies in that area focusing on improvement of efficiencies of the reactor. The works on increasing reactor efficiency can be classified in three main parts based on the affecting factor type that are improvement of redox material properties, progressing design of reactor and achieving better working conditions. In the literature, several studies based on parametric thermodynamic analysis considering only thermodynamic models are performed to understand the factors affecting efficiency to improve operation conditions. The need for better understanding the chemical kinetics heat and mass transfer mechanism has increased since thermodynamic analysis is not sufficient to represent the true nature of thermochemical cycle. However, there are limited number of studies combining transient nature of model that are reaction kinetics, heat, mass transfer mechanism and thermodynamic efficiency model to find optimum values for reactor and these studies are all simulation based studies.

Operation conditions such as working temperatures or heating time are important factors revealing trade-offs for reactor efficiency in a thermodynamic point of view as stated in many studies mentioned in previous section. However, no equation-based optimization research to find local optima via optimization methods with the aim of optimizing operating conditions of such solar thermochemical systems based on transient model considering heat, mass transfer mechanism and chemical kinetics has been found in the literature review, hence the objective of this thesis.

# CHAPTER 3

# PROBLEM DEFINITION

The scope of this study is to introduce a solution approach to the realistic representation of the energy efficiency and yield optimization problem of the solar thermochemical water splitting reaction system. In this chapter, it is aimed to describe the current situation of the solar thermal water splitting reactor system, identify the energy efficiency problem related to this system and analyse its components.

In Section 3.1, a simplified, general version of macro-scale model for one channelled monolith reactor is designed in the light of some assumptions, and then, in Section 3.2, process, its components and their relevance are analysed by constructing an influence diagram in order to formulate mathematical model of the energy efficiency optimization problem with ease.

## 3.1 System Description

In this part, a simplified model of one-channel monolith reactor for the solar thermochemical water splitting reaction is constructed and analysed.

### 3.1.1 Modeling and Analysis of the Physical Situation of Solar Thermochemical Water Splitting Reactor

Aforementioned solar thermochemical water splitting systems can be regarded as consisting of many cycles combining two sequential main steps: Reduction (Decomposition) step and oxidation step as shown in Section 2.1.1. With the aim of modeling of this two-step reaction system that takes place in a monolith reactor with one-channel, basic representation of the reaction is demonstrated below:

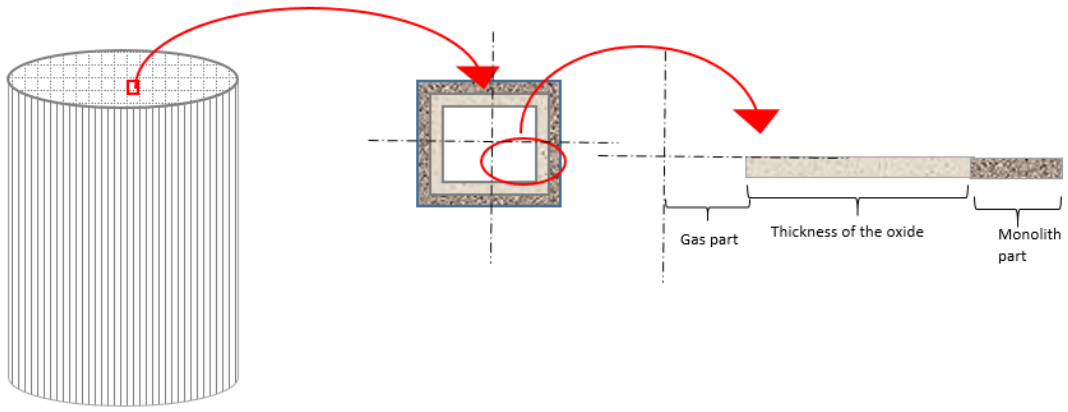


**Figure 3:1** A basic representation of monolith reactor and channel surface coated with redox material

In the literature, Agrafiotis et al [27] defined as the reaction kinetics for monolith reactor and surface coverage as below:

$$\Psi \frac{\mathrm{d}y}{\mathrm{d}t} = R_{\text{splitting}} - R_{\text{regeneration}}$$

$$R_{\text{splitting}} = \Psi k_{\text{lo}} c_1 (1 - y) \tag{3.1}$$

$$R_{\text{regeneration}} = \Psi k_{\text{reg}} y$$

where $\Psi$ represents total site number in monolith surface

y is the fraction of the surface coverage

$c_1$ is water concentration in the feed

Regeneration stands for reduction step and splitting stands for oxidation step.

Therefore, in the light of the literature review, modelling of the physical system is completed by defining required mass and energy conservation equations for both of the two step separately. Figure 3:2 and Figure 3:3 are the basic illustrations of the thermochemical steps showing system boundaries for the selected redox material, i.e.$CeO_2$.

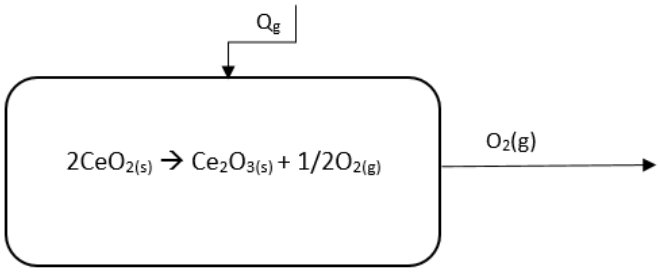


**Figure 3:2** Schematic of the reduction (decomposition) step

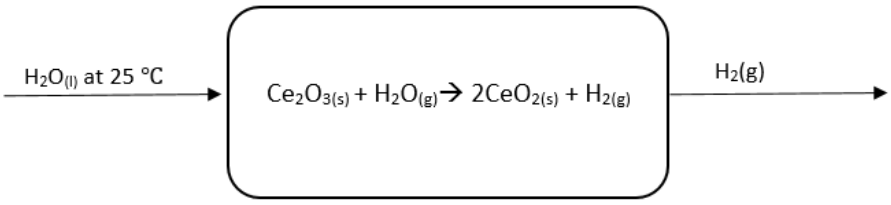


**Figure 3:3** Schematic of the oxidation step

#### 3.1.1.1 Mass Conversion Equations in Reduction Stage

**Oxygen generation rate:**

$$\dot{n}_{O_2} = \frac{dn_{O_2}}{dt} = A \cdot r_{desorption} \tag{3.2}$$

Oxygen desorption rate:

$$r_{desorption} = k_{red} N_{O*}^2 \tag{3.3}$$

$$k_{red} = k_{c,red} e^{(\frac{-Ea_{red}}{R \cdot T})} \tag{3.4}$$

where $k_{red}$is the reduction rate constant.

#### 3.1.1.2 Energy Conservation Equations in Reduction Stage

For the monolith channel, energy balance for gas phase with no spatial changes are modeled for reduction step as below:

$$\frac{d}{dt}(n_{O_2} c_{p,O_2} T) = \dot{Q}_{Loss(red)} + \dot{Q}_{sun} + A \cdot \Delta H_f \cdot r_{desorption} \tag{3.5}$$

#### 3.1.1.3 Mass Conversion Equations in Oxidation Stage

$$\dot{n}_{H_2} = \frac{dn_{H_2}}{dt} = 2 * A \cdot r_{wsp} \tag{3.6}$$

Rate of water splitting:

$$r_{wsp} = k_{wsp} P_{H2O} N_v \tag{3.7}$$

$$k_{wsp} = k_{c,wsp} e^{(\frac{-Ea_{wsp}}{R \cdot T})} \tag{3.8}$$

where $k_{wsp}$ is the water splitting rate constant

#### 3.1.1.4 Energy Conservation Equations in Oxidation Stage

For the monolith channel, energy balance for gas phase with no spatial changes are modeled for oxidation step in Equation 3.9.

$$\frac{d}{dt}(n_{H_2O}c_{p,H_2O}T) + \frac{d}{dt}(n_{H_2}c_{p,H_2}T) = \dot{Q}_{Loss(ox)} + A \cdot \Delta H_f \cdot r_{adsorption} \quad (3.9)$$

## 3.2 Problem Definition

### 3.2.1 Influence Diagram

By using influence diagrams systems are separated into its components for a specific performance measure such that a mathematical model can be created. A relationship diagram for two-step thermochemical system is shown in Figure 3:4, where the performance measure is represented by elliptic blocks while the decision variables (controllable variables) are symbolized by square blocks, uncontrollable variables or parameters are represented by the blocks that have cloud shapes.

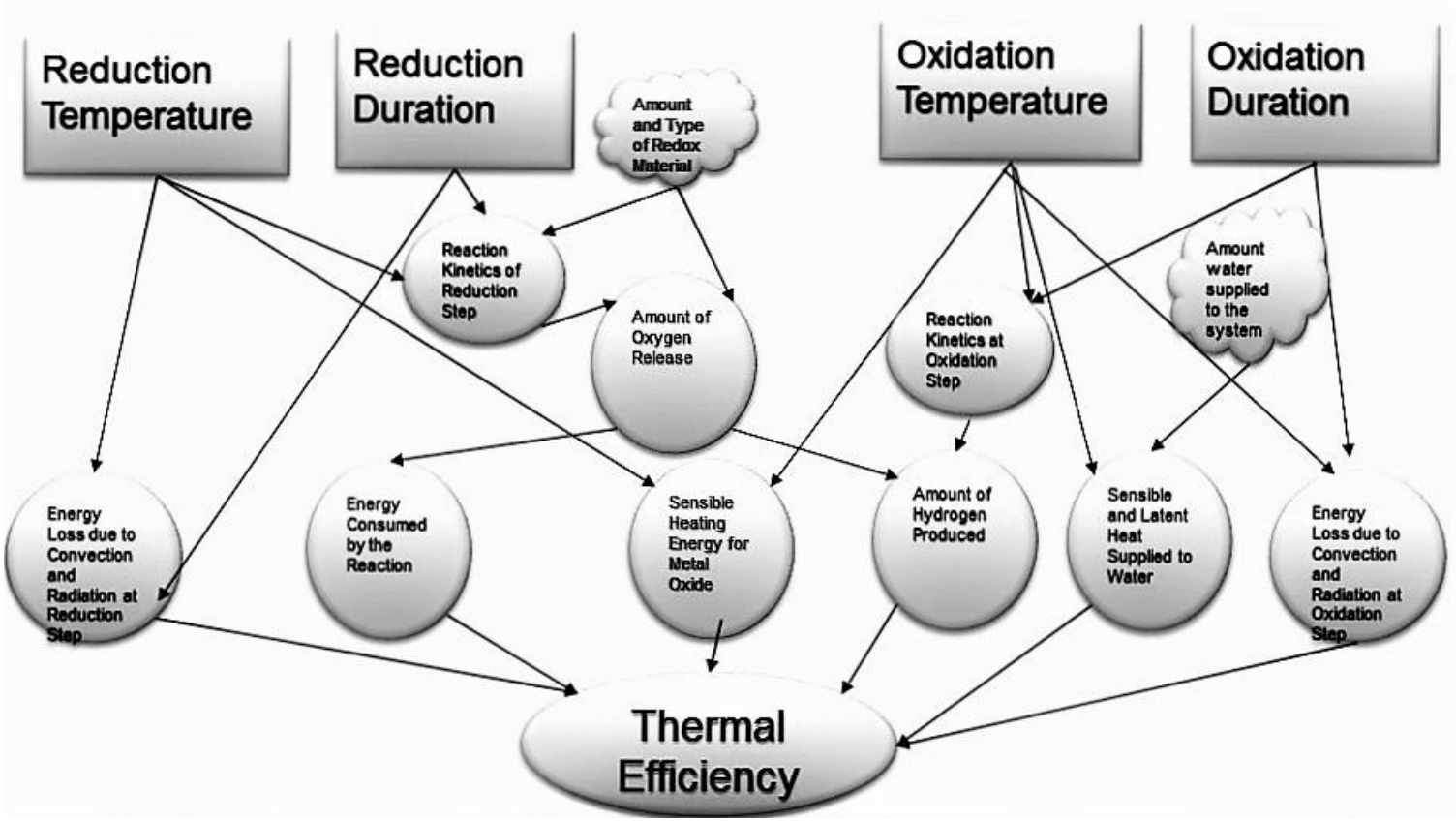


**Figure 3:4** Influence diagram of the two-step thermochemical water splitting cycle

### 3.2.2 Performance Measures

In the thermodynamic analysis of two-step thermochemical water splitting cycle although the energy efficiency is the main performance criteria as indicated in Chapter 2, many different performance measures can be defined in terms of the aspects that are intended to emphasize. In all energy efficiency definitions, the energy supplied to the system and energy obtained by the system can be comprised of different terms. In the thesis, the energy efficiency of the cycle is also described as below:

$$\eta = \frac{Energy\ obtained\ by\ the\ system}{Energy\ supplied\ to\ the\ system} = \frac{\dot{n}_{H_2} \times HHV}{\dot{Q}_{total}} \quad (3.9)$$

The term $\dot{Q}_{total}$, rate of energy supplied to the cycle can be expressed as the total of the following terms:

$\dot{Q}_{reheat}$ defined in Equation 3.10 is the rate of the sensible heat supplied to the redox material in order to reheat the material from oxidation temperature to reduction temperature between the following cycles. $\varepsilon_s$ represents the fraction of the heat recuperation to increase the energy efficiency.

$$\dot{Q}_{reheat} = \dot{n}_{CeO_2}(1 - \varepsilon_s)(\int_{T_C}^{T_H} c_{p_{CeO_2(s)}} dT) \quad (3.10)$$

$\dot{Q}_{Reaction,red}$ is another performance measure that is the rate of total energy consumed by the reduction process as shown below:

$$\dot{Q}_{Reaction,red} = (\dot{n}_{H_2})(\Delta H_{red}(T_H)) \quad (3.11)$$

Another performance measure, $\dot{Q}_{Loss}$, is the rate of heat loss due to re-radiation and convection shown by Equation 3.12:

$$\dot{Q}_{Loss} = \dot{Q}_{Loss(red)} + \dot{Q}_{Loss(ox)} \quad (3.12)$$

$\dot{Q}_{Loss(red)}$ is the rate of energy loss by convection and radiation at the reduction step demonstrated by equations set in Equation 3.13

$$\dot{Q}_{Loss(red)} = \dot{Q}_{con(red)} + \dot{Q}_{rad(red)}$$
$$\dot{Q}_{con(red)} = A_r \times h \times (T - T_a) \quad (3.13)$$
$$\dot{Q}_{rad(red)} = \sigma \times A_r \times (T^4 - T_a^4)$$

$\dot{Q}_{Loss(ox)}$ is the rate of energy loss by convection and radiation at the oxidation step.

$$\dot{Q}_{Loss(ox)} = \dot{Q}_{con(ox)} + \dot{Q}_{rad(ox)}$$

$$\dot{Q}_{con(ox)} = A_r \times h \times (T - T_a) \quad (3.14)$$
$$\dot{Q}_{rad(ox)} = \sigma \times A_r \times (T^4 - T_a^4)$$

$\dot{Q}_{water}$ is another performance measure that determines the rate of total energy supplied to the system. It is the rate of the sensible and latent heat consumed by the water given by Equation 3.15.

$$\dot{Q}_{water} = \dot{n}_{H_2O}\left[\Delta H_{H_2O(l)\rightarrow(g)}^{298K\rightarrow373K}\right] + \dot{n}_{H_2O}\left[\int_{373\,K}^{T_C} c_{p_{H_2O(g)}} dT\right] \quad (3.15)$$

### 3.2.3 Decision Variables

Operation temperatures (T) and durations ($\tau$) are the selected decision parameters that can be controlled.

The system accommodates many trade-offs on performance measures resulted by decision variables. For example, as the reduction temperatures and durations increases, the amount of hydrogen produced also increases. However, while the rise in reduction temperatures and durations occurs, heat losses due to re-radiation and convection also increase. For instance, another trade-off is that for the oxidation stage an increase in the oxidation temperature both result in a decrease in the amount of hydrogen produced and a decrease in the energy required to reheat the redox material as shown in Figure 3.5.

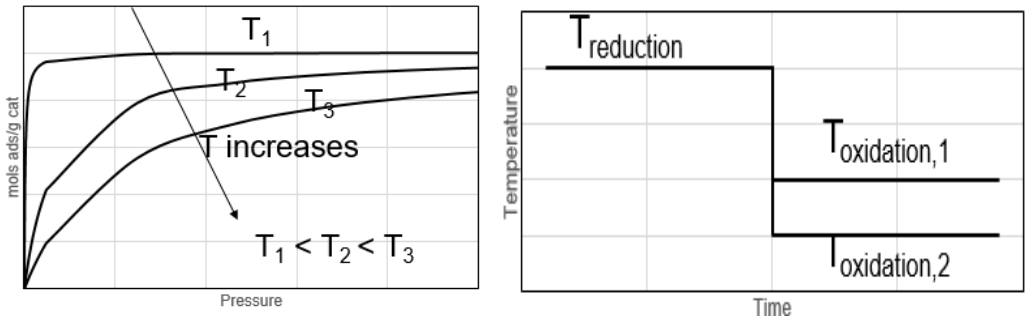


**Figure 3:5** Langmuir adsorption isotherm and energy required to reheat the redox material

### 3.2.4 Parameters

**Table 3:1** Parameters and their values obtained by the literature review

| Symbol | Definition | Value (unit) |
|---|---|---|
| $\boldsymbol{\varepsilon_s}$ | Heat recuperation by solid system | 0 |
| $\boldsymbol{c_{p_{CeO_2(s)}}}$ | Specific heat of the redox material | 143 (J/mol/K)[63] |
| $\boldsymbol{\Delta H_{red}(T_H)}$ | Enthalpy of the reduction process | 380900 (J/mol) |
| $\boldsymbol{P_{H_2O}}$ | Partial pressure of the steam | 100000 (Pa) |
| h | Free convective heat transfer coefficient | 20 (W/m. K) |
| $\boldsymbol{T_a}$ | Ambient air temperature | 298 (K) |
| $\boldsymbol{n_{CeO_2}}$ | Number of moles of redox material loaded to monolith | 0.2 (moles) |
| $\boldsymbol{\sigma}$ | Stefan Boltzman constant | $5.670373\times10^{-8}$ ($W/m^2/K^4$) |
| A | Surface area where adsorption takes place | 1 ($m^2$) |
| $\boldsymbol{A_r}$ | Effective surface area where the heat loss occurs | $3.14\times 10^{-6}$ ($m^2$) |
| R | Gas Constant | 8.314 (J/mol/K) |

**Table 3:2** (cont'd)

| Symbol | Definition | Value (unit) |
|---|---|---|
| $\boldsymbol{\varphi}$ | Maximum(allowable) storage capacity of the wall | 0.1 (mol/$m^2$) [27] |
| $\boldsymbol{k_{c,wsp}}$ | Rate constant for oxidation step | 35 ($m^3$/mol/s) [27] |
| $\boldsymbol{k_{c,red}}$ | Rate constant for reduction step | 1000000 (1/s) [27] |
| $\mathbf{Ea_{red}}$ | Activation energy of reduction step | 240000 (J/mol) [27] |
| $\mathbf{Ea_{wsp}}$ | Activation energy of reduction step | 100000 (J/mol) [27] |

# CHAPTER 4

# RESULTS AND DISCUSSIONS

In this chapter, the solution methods and required tools for the problem of determining optimum temperatures, and durations for the solar thermal water splitting process are explained, and mathematical formulations of the solution models are presented with their results. In the Section 4.1, methodologies for the solution of the problem is introduced in order to determine optimum working temperatures and cycle time for given system that maximizes energy efficiency and yield. The optimization models and parametric study formulations are explained in Section 4.2. Computational results of the solution algorithms and discussions related to these results are in extent of Section 4.3.

## 4.1 Solution Approach

In the light of the results of literature review, first a parametric analysis is conducted to see the effects of temperature change and process time change on different performance measures in order to solve the stated problem. In Section 4.1.1, the required tools and methods for the parametric analysis is explained in detail. Another solution approach that is dynamic optimization method for the solution of the optimization of working conditions to increase the efficiency of the cycle is presented in Section 4.1.2.

### 4.1.1 Thermodynamic Parametric Analysis

Parametric analysis approach is a way of understanding the general behaviour of the system response with respect to changes in any parameter. Most of the literature work presented in the solar thermochemical hydrogen production field related to thermodynamic cycle efficiency are parametric studies showing the parameter profiles[59]. General behaviour of several system variables and their performance measure trend lines can be investigated with this method by changing different parameters once at a time or simultaneously.

#### 4.1.1.1 Design of Experiments (DOE)

Design of experiments is a statistical method to screen multiple parameters (factors) in terms of their effects on the performance measure (output) and their interactions. It is also way of finding the optimum critical factors that maximize the output. In DOE, different approaches for example factorial design or surface response design can be used to evaluate the relation between factors (experiment conditions) and output (performance measure). Factorial design approach is usually applied to screen the multifactors to find critical factors, while the surface response design is used for determining optimum factor values in order to optimize the output. In factorial design, experiments with multiple combination of the possible values (levels) of the different parameters (factors) are designed and the variation in factors and output for each different case are investigated. The number of experiments (run) are determined by number of factor and their levels. For example, for three factor with two levels, at least $2^3$ experiments should be conducted to show main and interaction effects of the factors.

#### 4.1.1.2 Tools

**MATLAB**

MATLAB is a fourth generation numerical programming language platform that enables computational and graphical solutions for engineering problems. In this

thesis, all computational calculations of alternative scenarios are evaluated by means of MATLAB 9.0.0(R2016a) in computer with CPU @ 2.60 GHz and 32 GB RAM.

**MINITAB AND JMP**

Design of experiment part of the problem is carried out by means of both MINITAB and JMP, statistical analysis tools. Full factorial analysis is conducted on MINITAB 17 and JMP 12.0.1.

### 4.1.2 Mathematical Optimization Method

Problem is classified based on the descriptions in Engineering Optimization: Theory and Practice[64]. The classification of the problem is demonstrated in Table 4:1.

**Table 4:1** Classification of the Energy Efficiency Optimization Problem (modified from [64])

| Classification | The problem is |
|---|---|
| Unconstrained/Constrained | Constrained |
| Nature of the Design Variables | Dynamic |
| Nature of the Equations | Nonlinear |
| Deterministic /Stochastic Variables | Deterministic |
| Number of Objective Functions | Multi objective |

A nonlinear dynamic optimization problem bounded by both differential and algebraic equation systems. Therefore, direct-simultaneous dynamic optimization method is adopted as solution approach for the determination of local optima.

General form of the dynamic optimization problem with inequality and equality constraints is given below [65]:

$$min_{z(t),y(t),u(t),t_f,p} \quad \delta\left(z\left(t_f\right), y\left(t_f\right), u\left(t_f\right), t_f, p\right) \tag{4.1}$$

s.t. differential algebraic equation model:

$$\frac{dz}{dt} = f(z(t), y(t), u(t), t, p), \qquad z(0) = z_o \tag{4.2}$$

$$g(z(t), y(t), u(t), t, p) = 0 \tag{4.3}$$

Boundary conditions

$$\begin{aligned} z^L \leq z(t) \leq z^U \\ y^L \leq y(t) \leq y^U \\ u^L \leq u(t) \leq u^U \\ p^L \leq p \leq p^U \\ {t_f}^L \leq t_f \leq {t_f}^U \end{aligned} \tag{4.4}$$

where

$\delta$ represents objective function

$z$ stands for differential state variables

$y$ represents algebraic state variables

$u$ represents control state variables

$p$ stands for time invariant parameter.

f is the differential constraint

g is the algebraic constraint.

Figure 4:1 demonstrates the steps of the direct-simultaneous solution approach algorithm, that is adopted for the solution of the optimization problem

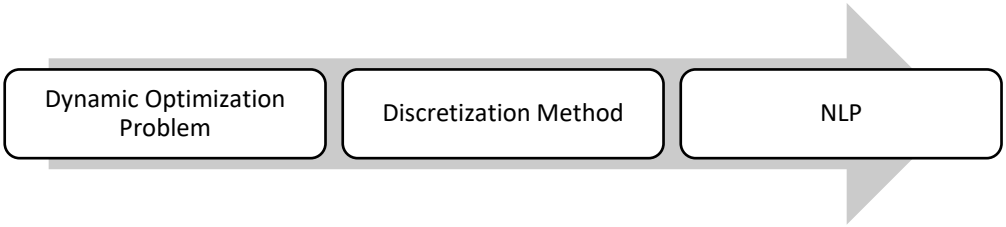


**Figure 4:1** Main steps of direct-simultaneous dynamic optimization method

#### 4.1.2.1 Discretization Method: Collocation Methods

The continuous time problem profiles are approximated to a family of polynomials on finite elements so that the problem is expressed as an NLP[66].

#### 4.1.2.2 Nonlinear Programming (NLP)

For the solution of NLP subproblems obtained by the discretization of general problem, several solvers using methods such as successive quadratic programming (SQP) and generalized reduced gradient (GRG) are used. Successive Quadratic Programming (SQP) is used to set a search path and a step size for next iteration by NLP problems and solves series of quadratic programming subproblems. The constraints and objective functions of the subproblems are derived from linearization of the constraints of the initial problem and quadratic approximation of the Lagrangian function, respectively[67]. However, highly constrained nonlinear programming problems require special techniques such as generalized reduced gradient algorithm which decreases apparent dimensionality of the optimization problem. The algorithm uses equality constraints instead of inequality constraints and reduces the complexity of the computations and number of the variables[68].

#### 4.1.2.3 Tools

**GAMS (General Algebraic Modeling System)**

General Algebraic Modeling System (GAMS), a mathematical optimization tool, is used for evaluating the local solutions of large NLP problems obtained as the result of the discretization of general differential-algebraic problem. GAMS incorporates several NLP solvers such as such as CONOPT, MINOS, SNOPT based on different NLP algorithms. For example, CONOPT and MINOS uses nested and gradient projection NLP algorithm code, while SNOPT operates sequential quadratic programme (SQP) algorithm code [65]. In the thesis, NLP problem for material requirement optimization problem is run via CONOPT, MINOS, and SNOPT in order to their compare local optimum solutions and execution times.

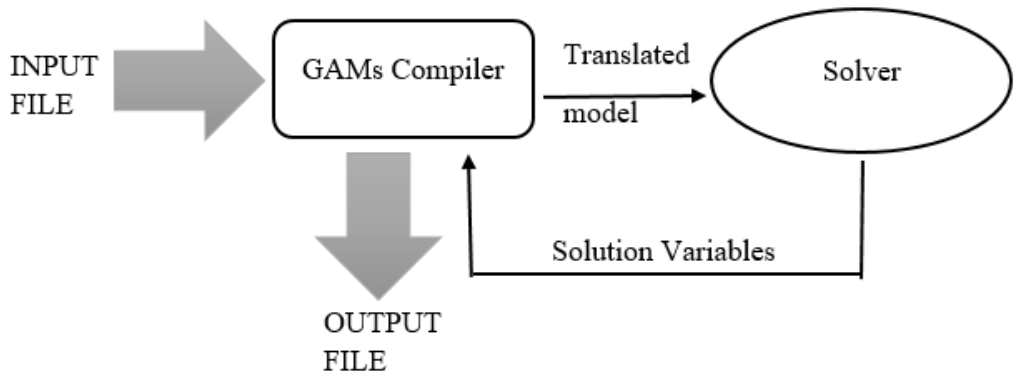


**Figure 4:2** The System of GAMS [69]

## 4.2 Mathematical Formulation

### 4.2.1 Formulation of Parametric Analysis

A heuristic algorithm whose steps are shown in Table 4:2 is formed and applied to see which parameter is more important in terms of their effects on efficiency of the cycle. Moreover, alternative scenarios are formed to see the effects of the specific parameters on different performance measures stated in Section 3.2.

**Table 4:2** Main steps of thermodynamic parameter analysis algorithm

| | **Steps** |
|---|---|
| **Step 1** | Creating a model to evaluate all of the performance measures for a specified input for the stated time range and temperature profile in MATLAB |
| **Step 2** | Creating alternative scenarios for different conditions based on the statistical approach (Design of Experiment) |
| **Step 3** | Simulating alternative scenarios in MATLAB code |
| **Step 4** | Estimating the main and interaction effects of factors in the design for different performance measures (Screening step) |
| **Step 5** | Determining the optimum working conditions for detected critical factors that maximizes the performance of the output (Optimization step) |

**Step 1. Creating the thermodynamic analysis model**

A MATLAB code presented in Appendix A for a given temperature profile is written to evaluate all of the performance measures stated in Section 3.2. To construct temperature profile approximately representing the general behaviour of the energy balances of the system, cycle time is divided into four parts. In part one called Reduction I in Figure 4:3, it is assumed that temperature increases from oxidation temperature to reduction temperature with a constant heating rate. In part two, reduction temperature is assumed to be constant. At the end of the part two, reduction process is completed. Then, system temperature starts to decrease gradually and linearly up to oxidation temperature. In the last part, temperature follows a constant pattern.

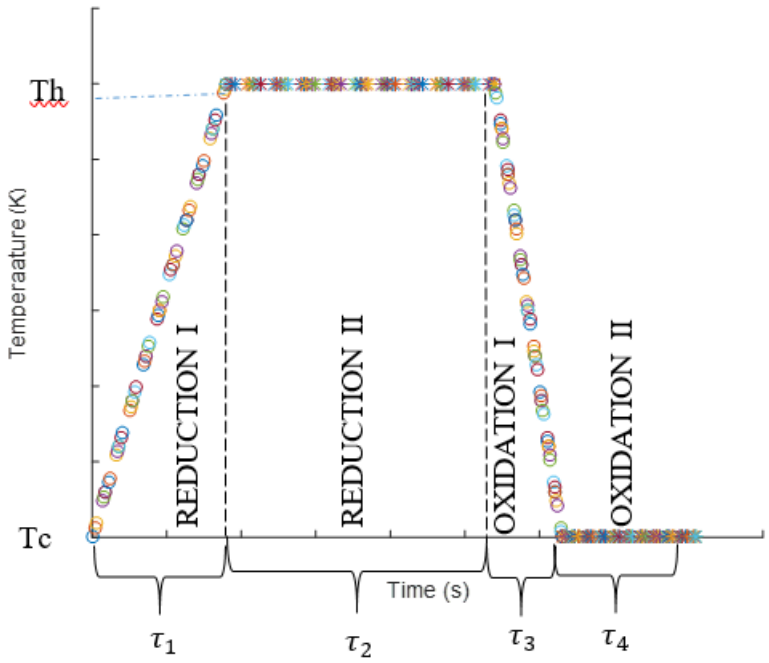


**Figure 4:3** Representative temperature profile example for two-step water splitting cycle model

In Figure 4:3, $\tau_i$ represents the required duration for each part i. For each discrete part, amount of hydrogen produced is evaluated by surface coverage equation and first order reaction kinetics. Also, all other performance measures stated in 3.2 are estimated in the model. MATLAB code for the model is presented in Appendix A.

**Step 2. Creating alternative scenarios to screen**

Alternative scenarios are created to screen multiple factors factorial design method is applied. Full factorial design is formed by selecting two temperatures -reduction and oxidation temperatures- and four durations as the important factors for screening process. Full factorial design conditions of alternative scenarios are demonstrated in Table 4:3 for better understanding of the concept.

**Table 4:3** Full factorial design of experiments

| Factor Name | Levels | Level Unit | Level Values | | | |
|---|---|---|---|---|---|---|
| **Reduction Temperature** | 4 | K | 900 | 1000 | 1100 | 1200 |
| **Delta T ($\Delta T$)** | 4 | K | 50 | 100 | 150 | 200 |
| **Reduction Time 1** | 4 | s | 300 | 600 | 900 | 1200 |
| **Reduction Time 2** | 4 | s | 300 | 600 | 900 | 1200 |
| **Oxidation Time 1** | 4 | s | 300 | 600 | 900 | 1200 |
| **Oxidation Time 2** | 4 | s | 300 | 600 | 900 | 1200 |

**Step 3. Simulation of the alternative scenarios**

Generated MATLAB code is run for several alternative scenarios with different working conditions to estimate different performance measures. For example, 4096 simulations are done in full factorial design for six factors with four levels.

**Step 4. Estimating the main and interaction effects**

By using factorial design properties, main and the interaction effects of factors are estimated and critical factors are determined as the result of the screening process.

**Step 5. Optimization step**

For the determined critical factors, statistical study is conducted by analysing the profilers of the critical factors and ranges for optimum values are estimated for these critical factors.

### 4.2.2 Mathematical Optimization Method

#### 4.2.2.1 Formulation for Constant Temperature Conditions

As a simplified solution approach, a nonlinear system optimization problem with constant temperature conditions is designed to evaluate optimum working temperatures for the given reduction and oxidation durations.

A model is created for water splitting reaction with a redox material that;

- Maximizes the thermal efficiency by
  - maximizing the hydrogen energy produced
  - minimizing the energy supplied to the system (reheating + energy for reaction)
- Considers reaction kinetics and dynamics

By determining the optimum working temperatures for given working durations.

**Assumptions**

Following assumptions are done in order to simplify the system:

- Temperature is assumed to be constant with respect to time and position during each step.

- Contrary to the parametric analysis model explained in previous section, temperature profile is thought as two discrete parts: Oxidation and reduction steps
- Only two performance measures energy required for reaction and energy spent on reheating are considered.
- Inside of the channel of a monolith is a uniform system with no axial and radial changes in temperature or concentration of materials with respect to position.
- First order reaction mechanism is assumed.
- Redox material properties and gas properties such as heat capacities are constant.
- Gas flow is laminar.
- Pressure throughout the monolith channel is constant, since pressure drop is small in the channel and it can be neglected.

**Performance Measures**

In this basic model, energy efficiency defined in Equation 3.5 is the performance criterion. However, $\dot{Q}_{total}$, energy supplied to the cycle is assumed to be total of the only the sensible heat supplied to the redox material, and energy consumed by the endothermic process. Other components are neglected for simplification.

**Decision Variables and Parameters**

Reduction and oxidation temperatures are the main decision variables of the system. Parameters gathered from the literature review shown in Section 3.2.3 are valid and used in the model.

**Constraints**

System is bounded by surface coverage equation and first order kinetics for each discrete step.

GAMS code for nonlinear system and constant temperature conditions are presented in Appendix B.

## 4.3 Results and Discussion

### 4.3.1 Parametric Analysis Results and Discussion

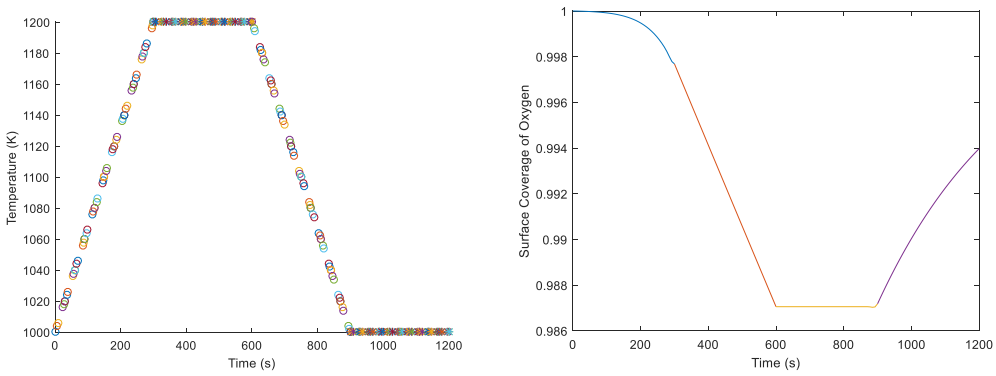


**Figure 4:4** Temperature profile and surface coverage of oxygen for temperature range 1000 K-1200 K for $\tau_1 = 300\ s$, $\tau_2 = 300\ s$, $\tau_3 = 300\ s$, $\tau_4 = 300\ s$

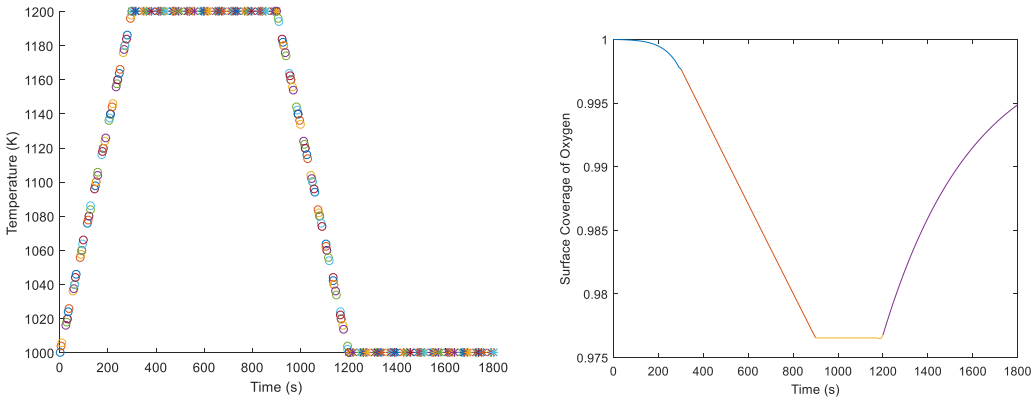


**Figure 4:5** Temperature profile and surface coverage of oxygen for temperature range 1000 K-1200 K for $\tau_1 = 300\ s$, $\tau_2 = 600\ s$, $\tau_3 = 300\ s$, $\tau_4 = 600\ s$

Figure 4:4 and Figure 4:5 demonstrates the temperature profiles and surface coverage of oxygen obtained as example outputs of the MATLAB. When the two graph are compared with each other, it can be said that as the time required for reduction and oxidation increases, the amount of the hydrogen produced also increases. This is an expected result in agreement with the aforementioned problem definition up to the point where redox material oxygen capacity is saturated. Since the energy given to the system also is increased with the increasing durations due to heat losses, more systematic approach is required in order to analyse the complete effects of the operation durations and temperatures. Therefore, full factorial analysis is conducted. The time required for reduction and oxidation are actually limited by the available material. Therefore, there will be a maximum time for reduction and maximum time for oxidation determined by the rates of reduction and oxidation respectively. In the absence of the accurate rate information, a parametric study is presented here.

#### 4.3.1.1 Total Efficiency of the Cycle

As mentioned in previous section, 4096 simulations were completed for the full factorial analysis of the system with six factors and four levels. First, a screening analysis was conducted to see the main effects and interactions of each factor. However, results of screening analysis concluded that the data showed non-normal behaviour and had singularities. Therefore, variability chart for total efficiency of the system was plotted to analyse the reasons why the data showed non-normal behaviour. Figure 4:6Figure 4:7 shows how the efficiency changes with respect to different values of reduction temperature and temperature difference-DeltaT- between reduction and oxidation temperature.

As can be seen from Figure 4:6 and Figure 4*:7*, total efficiency of the cycle is estimated as zero for the conditions both where reduction temperature equals to 900 K and temperature difference equals to 50, 100, 150 and 200 and where reduction temperature equals to 1200 K and temperature difference equals to 50, 100, and 150. The reason why total efficiency is calculated as zero for these conditions is that there are thermodynamic limitations for reduction and oxidation temperatures depending

on the nature of the redox material. For example, for this analysis, reduction occurs only between 1000 K and 1200 K, while the oxidation of the redox material is limited to temperature range of 900 K-1000 K. Therefore, when the temperature is equal to 900 K, no reduction reaction occurs for the selected redox material.

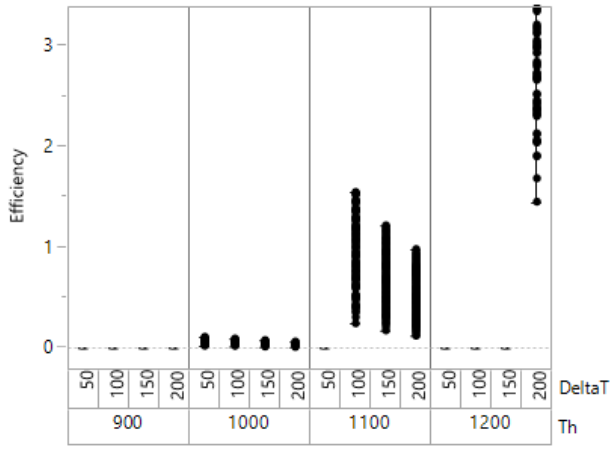


**Figure 4:6** Variability chart for total efficiency for full factorial analysis with six factors and four levels

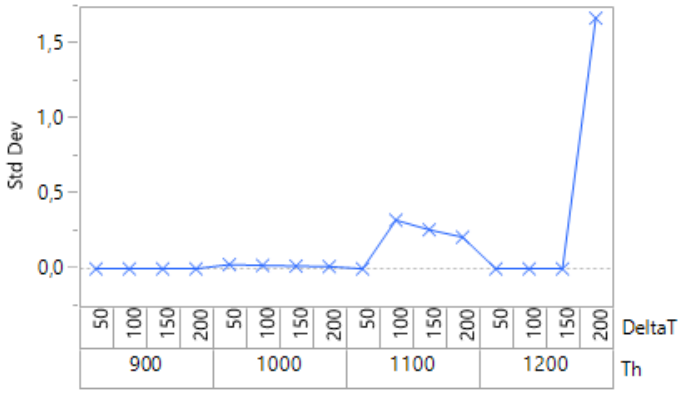


**Figure 4:7** Variability summary for total efficiency for full factorial analysis with six factors and four levels

All conditions where total efficiency was equal to zero were excluded from the analysis in order to eliminate singularities and non-normalities in the data. Figure 4:8Figure 4:9 show non-zero conditions for total efficiency. Rest of screening analysis are performed based on the non-zero conditions demonstrated on Figure 4:8Figure 4:9.

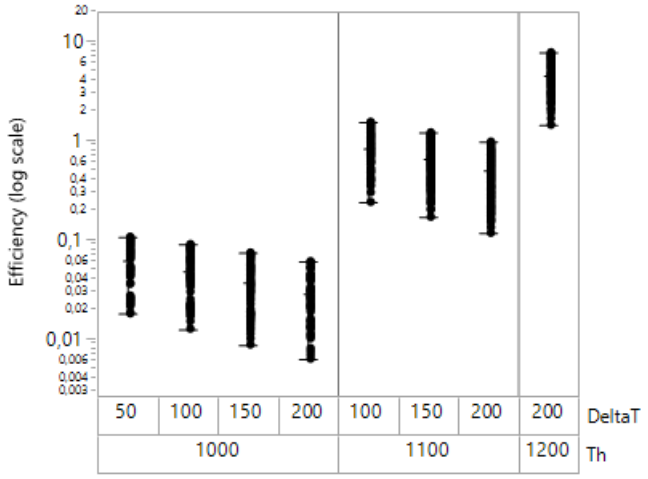


**Figure 4:8** Variability chart for total efficiency for cases where efficiency is non-zero

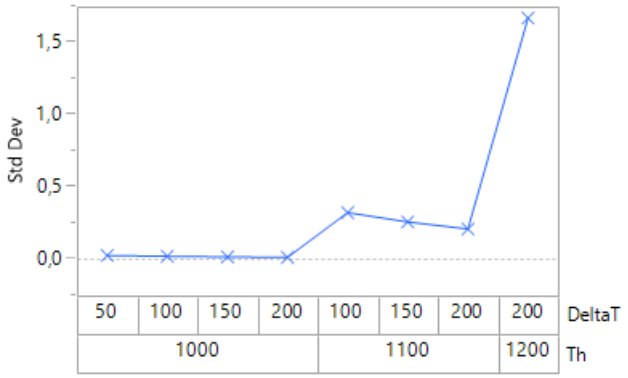


**Figure 4:9** Variability summary for total efficiency for cases where efficiency is non-zero

Table 4:4 shows the results of the main effects and interactions for total efficiency that are obtained by model fitting. Model fitting includes full factorial analysis up-to-degree three for linear effects and polynomial up-to-degree three for nonlinearities. In Table 4:4, factors or interactions having the probability values less than significance level of 0.05 are considered as statistically significant and indicated by star symbol(*). As can be seen from the Table 4:4, all of the six main factors and the interactions " Th*DeltaT", "Th*Reduction Time 1", "Th*Reduction Time 2", "Th*Oxidation Time 2", "Reduction Time 2*Oxidation Time 2", "Th*Th", and "Oxidation Time 2*Oxidation Time 2" are statistically significant in terms of total efficiency.

**Table 4:4** Summary of the main effects and interactions for total efficiency

| Source | Nparm | DF | Sum of Squares | F Ratio | Prob > F |
|---|---|---|---|---|---|
| Th | 1 | 1 | 581.9 | 7344.7 | <.0001* |
| DeltaT | 1 | 1 | 13.2 | 166.5 | <.0001* |
| Reduction Time 1 | 1 | 1 | 6.7 | 84.3 | <.0001* |
| Reduction Time 2 | 1 | 1 | 152.7 | 1926.8 | <.0001* |
| Oxidation Time 1 | 1 | 1 | 0.4 | 4.8 | 0.0284* |
| Oxidation Time 2 | 1 | 1 | 34.8 | 438.8 | <.0001* |
| Th*DeltaT | 1 | 1 | 7.0 | 88.2 | <.0001* |
| Th*Reduction Time 1 | 1 | 1 | 11.7 | 147.6 | <.0001* |
| DeltaT*Reduction Time 1 | 1 | 1 | 0.0 | 0.3 | 0.5956 |
| Th*Reduction Time 2 | 1 | 1 | 240.4 | 3034.3 | <.0001* |
| DeltaT*Reduction Time 2 | 1 | 1 | 0.3 | 3.7 | 0.0540 |
| Reduction Time 1*Reduction Time 2 | 1 | 1 | 0.1 | 1.1 | 0.2861 |
| Th*Oxidation Time 1 | 1 | 1 | 0.0 | 0.4 | 0.5467 |
| DeltaT*Oxidation Time 1 | 1 | 1 | 0.1 | 1.6 | 0.2109 |
| Reduction Time 1*Oxidation Time 1 | 1 | 1 | 0.0 | 0.0 | 0.9091 |
| Reduction Time 2*Oxidation Time 1 | 1 | 1 | 0.1 | 0.8 | 0.3835 |
| Th*Oxidation Time 2 | 1 | 1 | 65.8 | 830.5 | <.0001* |
| DeltaT*Oxidation Time 2 | 1 | 1 | 0.0 | 0.0 | 0.8343 |
| Reduction Time 1*Oxidation Time 2 | 1 | 1 | 0.1 | 1.9 | 0.1701 |
| Reduction Time 2*Oxidation Time 2 | 1 | 1 | 3.1 | 38.7 | <.0001* |
| Oxidation Time 1*Oxidation Time 2 | 1 | 1 | 0.1 | 1.5 | 0.2237 |
| Th*Th | 1 | 1 | 640.3 | 8082.2 | <.0001* |
| DeltaT*DeltaT | 1 | 1 | 0.0 | 0.1 | 0.7696 |
| Reduction Time 1*Reduction Time 1 | 1 | 1 | 0.0 | 0.0 | 0.9116 |
| Reduction Time 2*Reduction Time 2 | 1 | 1 | 0.2 | 2.5 | 0.1113 |
| Oxidation Time 1*Oxidation Time 1 | 1 | 1 | 0.0 | 0.1 | 0.7303 |
| Oxidation Time 2*Oxidation Time 2 | 1 | 1 | 3.5 | 43.6 | <.0001* |

Figure 4:10 shows the actual by predicted plot for total efficiency. It can be concluded that fitted model shows less variation because of random effects for higher values of the total efficiency.

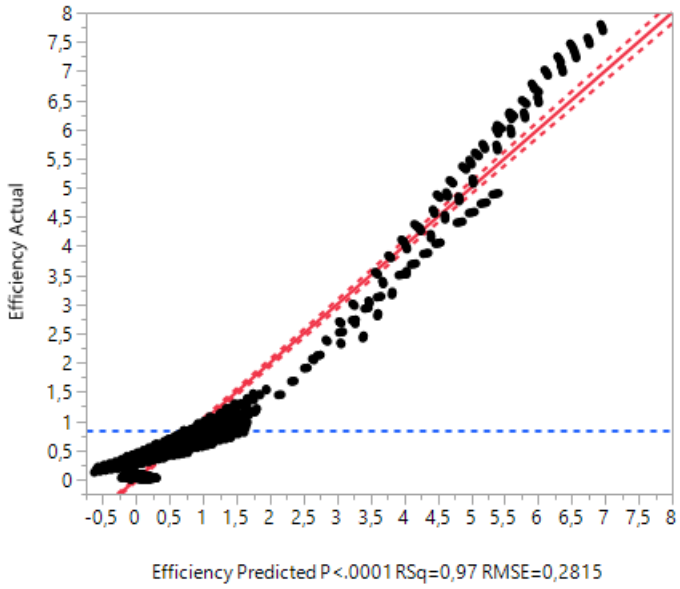


**Figure 4:10** Actual by predicted plot for total efficiency

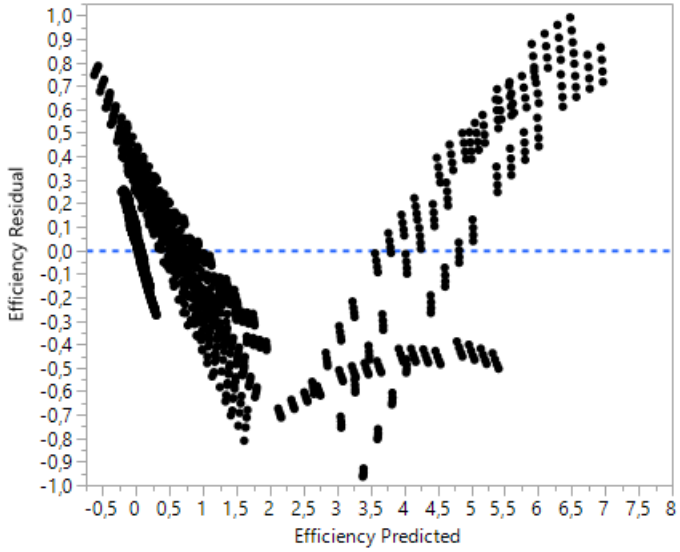


**Figure 4:11** Residual by predicted plot for total efficiency

Figure 4:11 demonstrates the residuals by predicted plot for total efficiency. From the graph, it can be concluded that there are large residuals and unequal variations in the analysis.

#### 4.3.1.2 Amount of the Hydrogen Produced

For amount of the hydrogen produced, except oxidation time 1, all of the main factors are statistically important. Besides, interactions "Th*DeltaT", "Th*Reduction Time 1", Th*Reduction Time 2", "Th*Oxidation Time 2", "DeltaT*Reduction Time 2", "Reduction Time 2*Oxidation Time 2", "Th*Th", and Oxidation Time 2*Oxidation Time 2" are significant in terms of amount of the hydrogen produced.

**Table 4:5** Summary of the main effects and interactions for amount of the hydrogen produced

| Source | Nparm | DF | Sum of Squares | F Ratio | Prob > F |
|---|---|---|---|---|---|
| Th | 1 | 1 | 0.0 | 3327.8 | <.0001* |
| DeltaT | 1 | 1 | 0.0 | 22.1 | <.0001* |
| Reduction Time 1 | 1 | 1 | 0.0 | 59.2 | <.0001* |
| Reduction Time 2 | 1 | 1 | 0.0 | 1211.6 | <.0001* |
| Oxidation Time 1 | 1 | 1 | 0.0 | 3.8 | 0.0504 |
| Oxidation Time 2 | 1 | 1 | 0.0 | 293.6 | <.0001* |
| Th*DeltaT | 1 | 1 | 0.0 | 11.6 | 0.0007* |
| Th*Reduction Time 1 | 1 | 1 | 0.0 | 116.0 | <.0001* |
| Th*Reduction Time 2 | 1 | 1 | 0.0 | 2225.4 | <.0001* |
| Th*Oxidation Time 1 | 1 | 1 | 0.0 | 0.2 | 0.6368 |
| Th*Oxidation Time 2 | 1 | 1 | 0.0 | 616.5 | <.0001* |
| DeltaT*Reduction Time 1 | 1 | 1 | 0.0 | 0.0 | 0.8491 |
| DeltaT*Reduction Time 2 | 1 | 1 | 0.0 | 12.5 | 0.0004* |
| DeltaT*Oxidation Time 1 | 1 | 1 | 0.0 | 0.7 | 0.3901 |
| DeltaT*Oxidation Time 2 | 1 | 1 | 0.0 | 1.6 | 0.2034 |
| Reduction Time 1*Reduction Time 2 | 1 | 1 | 0.0 | 0.0 | 0.9446 |
| Reduction Time 1*Oxidation Time 1 | 1 | 1 | 0.0 | 0.0 | 0.9012 |
| Reduction Time 1*Oxidation Time 2 | 1 | 1 | 0.0 | 2.0 | 0.1625 |
| Reduction Time 2*Oxidation Time 1 | 1 | 1 | 0.0 | 0.6 | 0.4539 |
| Reduction Time 2*Oxidation Time 2 | 1 | 1 | 0.0 | 38.2 | <.0001* |
| Oxidation Time 1*Oxidation Time 2 | 1 | 1 | 0.0 | 0.5 | 0.4923 |
| Th*Th | 1 | 1 | 0.0 | 5335.4 | <.0001* |
| DeltaT*DeltaT | 1 | 1 | 0.0 | 0.0 | 0.9466 |
| Reduction Time 1*Reduction Time 1 | 1 | 1 | 0.0 | 0.0 | 0.9952 |
| Reduction Time 2*Reduction Time 2 | 1 | 1 | 0.0 | 0.0 | 0.8985 |
| Oxidation Time 1*Oxidation Time 1 | 1 | 1 | 0.0 | 0.0 | 0.8423 |
| Oxidation Time 2*Oxidation Time 2 | 1 | 1 | 0.0 | 25.5 | <.0001* |

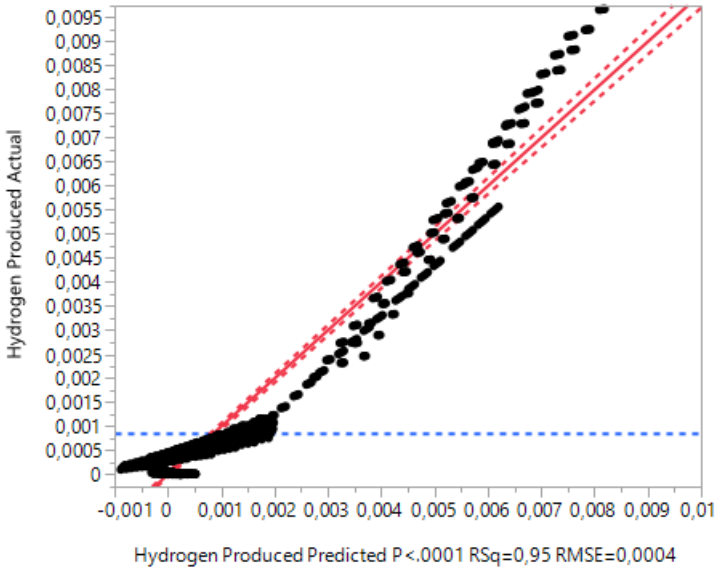


**Figure 4:12** Actual by predicted plot for amount of the hydrogen produced

Figure 4:12 shows actual by predicted plot for amount of the hydrogen produced. It can be said that goodness-of-fitting is better for higher values of amount of hydrogen produced.

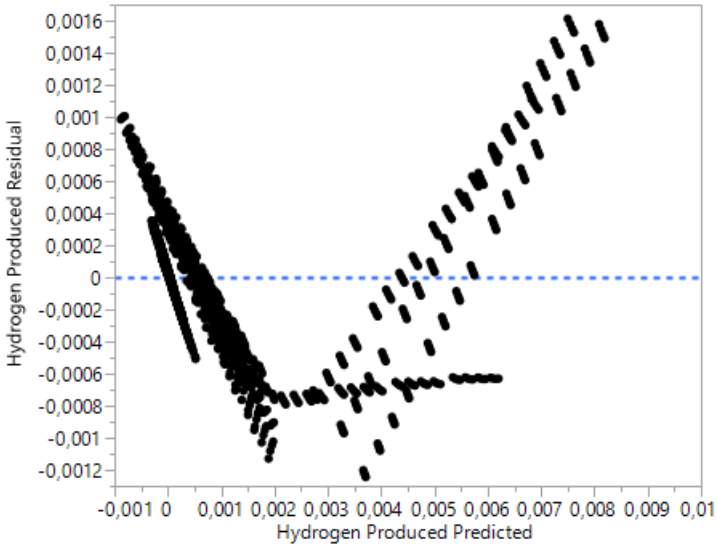


**Figure 4:13** Residual by predicted plot for amount of the hydrogen produced

Figure 4:13 shows there are large residuals and unequal variations in the analysis.

#### 4.3.1.3 Heat Loss due to Convection and Re-radiation

**Table 4:6** Summary of the main effects and interactions for total heat loss due to convection and re-radiation, $Q_{loss}$

| Source | Nparm | DF | Sum of Squares | F Ratio | Prob > F |
|---|---|---|---|---|---|
| Th | 1 | 1 | 25774831 | 3314926 | <.0001* |
| DeltaT | 1 | 1 | 2823715 | 363160.7 | <.0001* |
| Reduction Time 1 | 1 | 1 | 11127324 | 1431096 | <.0001* |
| Reduction Time 2 | 1 | 1 | 18003772 | 2315482 | <.0001* |
| Oxidation Time 1 | 1 | 1 | 11127324 | 1431096 | <.0001* |
| Oxidation Time 2 | 1 | 1 | 6524944 | 839179.3 | <.0001* |
| Th*DeltaT | 1 | 1 | 53293 | 6854.1 | <.0001* |
| Th*Reduction Time 1 | 1 | 1 | 541820 | 69684.1 | <.0001* |
| DeltaT*Reduction Time 1 | 1 | 1 | 53403 | 6868.2 | <.0001* |
| Th*Reduction Time 2 | 1 | 1 | 850436 | 109375.4 | <.0001* |
| DeltaT*Reduction Time 2 | 1 | 1 | 102 | 13.1 | 0.0003* |
| Reduction Time 1*Reduction Time 2 | 1 | 1 | 0.0 | 0.0 | 1.0000 |
| Th*Oxidation Time 1 | 1 | 1 | 541820 | 69684.1 | <.0001* |
| DeltaT*Oxidation Time 1 | 1 | 1 | 53403 | 6868.2 | <.0001* |
| Reduction Time 1*Oxidation Time 1 | 1 | 1 | 0.0 | 0.0 | 1.0000 |
| Reduction Time 2*Oxidation Time 1 | 1 | 1 | 0.0 | 0.0 | 1.0000 |
| Th*Oxidation Time 2 | 1 | 1 | 326669 | 42013.2 | <.0001* |
| DeltaT*Oxidation Time 2 | 1 | 1 | 170871 | 21975.9 | <.0001* |
| Reduction Time 1*Oxidation Time 2 | 1 | 1 | 0.0 | 0.0 | 1.0000 |
| Reduction Time 2*Oxidation Time 2 | 1 | 1 | 0.0 | 0.0 | 1.0000 |
| Oxidation Time 1*Oxidation Time 2 | 1 | 1 | 0.0 | 0.0 | 1.0000 |
| Th*Th | 1 | 1 | 213877 | 27506.9 | <.0001* |
| DeltaT*DeltaT | 1 | 1 | 8724 | 1122.0 | <.0001* |
| Reduction Time 1*Reduction Time 1 | 1 | 1 | 0.0 | 0.0 | 1.0000 |
| Reduction Time 2*Reduction Time 2 | 1 | 1 | 0.0 | 0.0 | 1.0000 |
| Oxidation Time 1*Oxidation Time 1 | 1 | 1 | 0.0 | 0.0 | 1.0000 |
| Oxidation Time 2*Oxidation Time 2 | 1 | 1 | 0.0 | 0.0 | 1.0000 |

For the performance measure, total heat loss due to convection and re-radiation, all of the six factors are significant as main effects. “Th*DeltaT”, “Th*Reduction Time 1”, “DeltaT*Reduction Time 1”, “Th*Reduction Time 2”, “DeltaT*Reduction Time 2”, “Th*Oxidation Time 1”, “DeltaT*Oxidation Time 1”, “Th*Oxidation Time 2”, “DeltaT*Oxidation Time 2”, “Th*Th”, and “DeltaT*DeltaT” are the statistically important interactions.

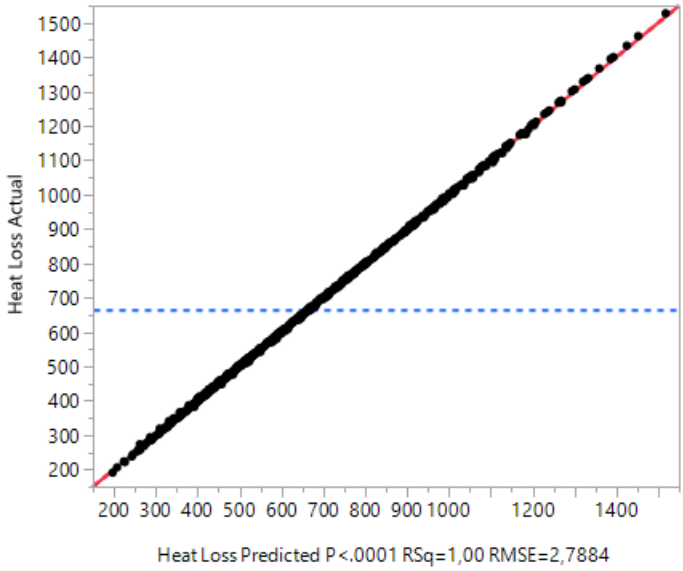


**Figure 4:14** Actual by predicted plot for total heat loss due to convection and re-radiation, $Q_{loss}$

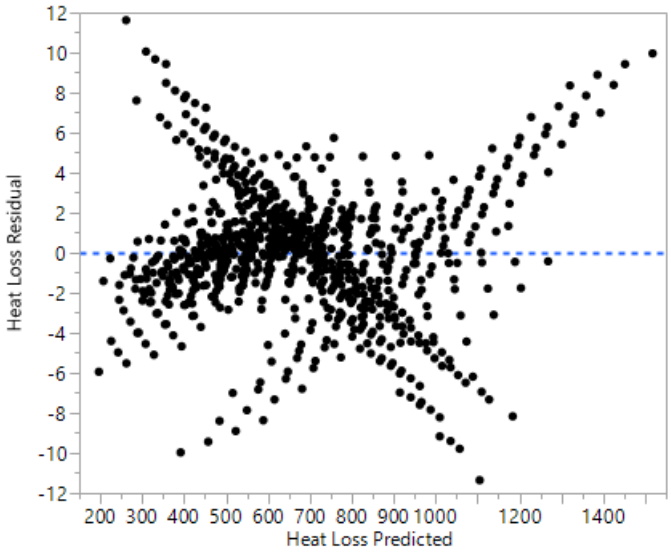


**Figure 4:15** Residual by predicted plot for total heat loss due to convection and re-radiation, $Q_{loss}$

Figure 4:14 shows no random effect while the Figure 4:15 demonstrates uneven distribution of the residuals.

#### 4.3.1.4 Energy Required to Reheat the Redox Material

Based on the Table 4:7, it can be concluded that only factor that have effects on the energy required for reheating the redox material is temperature difference between reduction and oxidation temperatures (DeltaT).

**Table 4:7** Summary of the main effects and interactions for the energy required for reheating the redox material, $Q_{reheat}$

| Source | Nparm | DF | Sum of Squares | F Ratio | Prob > F |
|---|---|---|---|---|---|
| Th | 1 | 1 | 0 | 0 | 1.0000 |
| DeltaT | 1 | 1 | 2308321764 | 9.78e+18 | <.0001* |
| Reduction Time 1 | 1 | 1 | 0 | 0 | 1.0000 |
| Reduction Time 2 | 1 | 1 | 0 | 0 | 1.0000 |
| Oxidation Time 1 | 1 | 1 | 0 | 0 | 1.0000 |
| Oxidation Time 2 | 1 | 1 | 0 | 0 | 1.0000 |
| Th*DeltaT | 1 | 1 | 0 | 0 | 1.0000 |
| Th*Reduction Time 1 | 1 | 1 | 0 | 0 | 1.0000 |
| DeltaT*Reduction Time 1 | 1 | 1 | 0 | 0 | 1.0000 |
| Th*Reduction Time 2 | 1 | 1 | 0 | 0 | 1.0000 |
| DeltaT*Reduction Time 2 | 1 | 1 | 0 | 0 | 1.0000 |
| Reduction Time 1*Reduction Time 2 | 1 | 1 | 0 | 0 | 1.0000 |
| Th*Oxidation Time 1 | 1 | 1 | 0 | 0 | 1.0000 |
| DeltaT*Oxidation Time 1 | 1 | 1 | 0 | 0 | 1.0000 |
| Reduction Time 1*Oxidation Time 1 | 1 | 1 | 0 | 0 | 1.0000 |
| Reduction Time 2*Oxidation Time 1 | 1 | 1 | 0 | 0 | 1.0000 |
| Th*Oxidation Time 2 | 1 | 1 | 0 | 0 | 1.0000 |
| DeltaT*Oxidation Time 2 | 1 | 1 | 0 | 0 | 1.0000 |
| Reduction Time 1*Oxidation Time 2 | 1 | 1 | 0 | 0 | 1.0000 |
| Reduction Time 2*Oxidation Time 2 | 1 | 1 | 0 | 0 | 1.0000 |
| Oxidation Time 1*Oxidation Time 2 | 1 | 1 | 0 | 0 | 1.0000 |
| Th*Th | 1 | 1 | 0 | 0 | 1.0000 |
| DeltaT*DeltaT | 1 | 1 | 0 | 0 | 1.0000 |
| Reduction Time 1*Reduction Time 1 | 1 | 1 | 0 | 0 | 1.0000 |
| Reduction Time 2*Reduction Time 2 | 1 | 1 | 0 | 0 | 1.0000 |
| Oxidation Time 1*Oxidation Time 1 | 1 | 1 | 0 | 0 | 1.0000 |
| Oxidation Time 2*Oxidation Time 2 | 1 | 1 | 0 | 0 | 1.0000 |

#### 4.3.1.5 Energy Required for Endothermic Reaction

For the energy required for endothermic reaction, except oxidation time 1, all of the main factors are statistically important. Besides, interactions "Th*DeltaT", "Th*Reduction Time 1", Th*Reduction Time 2", "Th*Oxidation Time 2", "DeltaT*Reduction Time 2", "Reduction Time 2*Oxidation Time 2", "Th*Th", and Oxidation Time 2*Oxidation Time 2" are significant in terms of the energy required for endothermic reaction.

**Table 4:8** Summary of the main effects and interactions for the energy required for the endothermic reaction, $Q_{reaction}$

| Source | Nparm | DF | Sum of Squares | F Ratio | Prob > F |
|---|---|---|---|---|---|
| Th | 1 | 1 | 79339809 | 3327.8 | <.0001* |
| DeltaT | 1 | 1 | 526237 | 22.1 | <.0001* |
| Reduction Time 1 | 1 | 1 | 1412005 | 59.2 | <.0001* |
| Reduction Time 2 | 1 | 1 | 28886621 | 1211.6 | <.0001* |
| Oxidation Time 1 | 1 | 1 | 91386 | 3.8 | 0.0504 |
| Oxidation Time 2 | 1 | 1 | 6998774 | 293.6 | <.0001* |
| Th*DeltaT | 1 | 1 | 276384 | 12.0 | 0.0007* |
| Th*Reduction Time 1 | 1 | 1 | 2765512 | 116.0 | <.0001* |
| DeltaT*Reduction Time 1 | 1 | 1 | 863 | 0.0 | 0.8491 |
| Th*Reduction Time 2 | 1 | 1 | 53057806 | 2225.4 | <.0001* |
| DeltaT*Reduction Time 2 | 1 | 1 | 297295 | 12.5 | 0.0004* |
| Reduction Time 1*Reduction Time 2 | 1 | 1 | 115 | 0.0 | 0.9446 |
| Th*Oxidation Time 1 | 1 | 1 | 5318 | 0.2 | 0.6368 |
| DeltaT*Oxidation Time 1 | 1 | 1 | 17616 | 0.7 | 0.3901 |
| Reduction Time 1*Oxidation Time 1 | 1 | 1 | 368 | 0.0 | 0.9012 |
| Reduction Time 2*Oxidation Time 1 | 1 | 1 | 13378 | 0.6 | 0.4539 |
| Th*Oxidation Time 2 | 1 | 1 | 14697823 | 616.5 | <.0001* |
| DeltaT*Oxidation Time 2 | 1 | 1 | 38598 | 1.6 | 0.2034 |
| Reduction Time 1*Oxidation Time 2 | 1 | 1 | 46549 | 2.0 | 0.1625 |
| Reduction Time 2*Oxidation Time 2 | 1 | 1 | 910181 | 38.2 | <.0001* |
| Oxidation Time 1*Oxidation Time 2 | 1 | 1 | 11246 | 0.5 | 0.4923 |
| Th*Th | 1 | 1 | 127203529 | 5335.4 | <.0001* |
| DeltaT*DeltaT | 1 | 1 | 107 | 0.0 | 0.9466 |
| Reduction Time 1*Reduction Time 1 | 1 | 1 | 0.9 | 0.0 | 0.9952 |
| Reduction Time 2*Reduction Time 2 | 1 | 1 | 388 | 0.0 | 0.8985 |
| Oxidation Time 1*Oxidation Time 1 | 1 | 1 | 944 | 0.0 | 0.8423 |
| Oxidation Time 2*Oxidation Time 2 | 1 | 1 | 607582 | 25.5 | <.0001* |

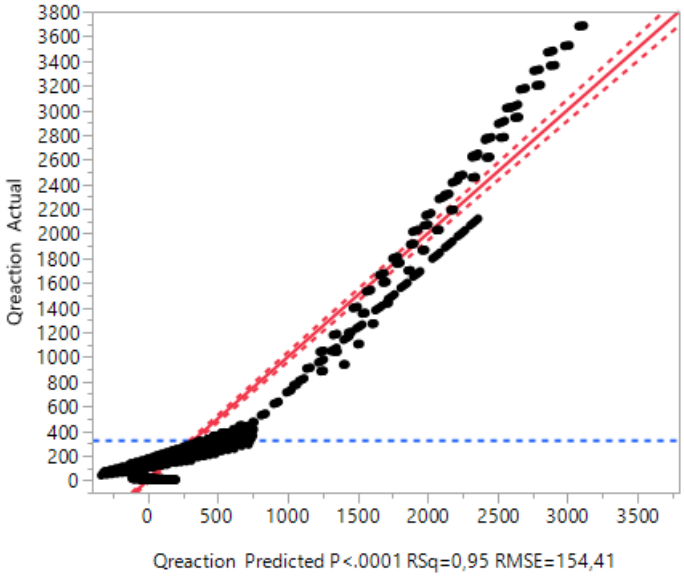


**Figure 4:16** Actual by predicted plot for the energy required for the endothermic reaction, $Q_{reaction}$

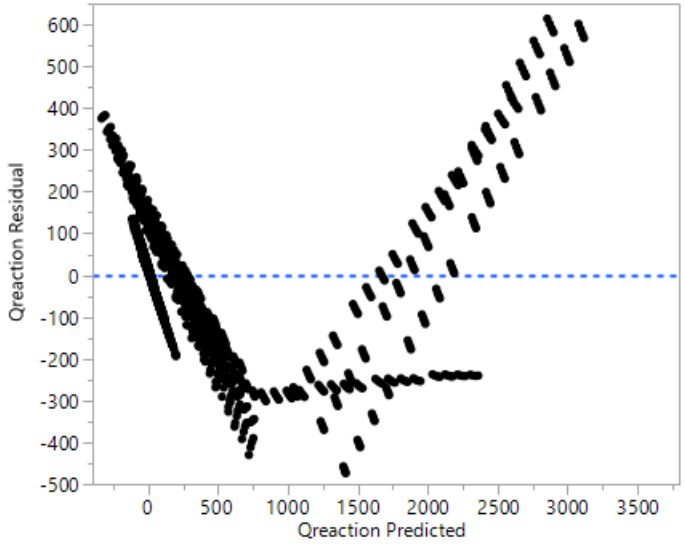


**Figure 4:17** Residual by predicted plot for the energy required for the endothermic reaction, $Q_{reaction}$

#### 4.3.1.6 Energy Spent on Heating the Water

Since oxidation temperature is the only decisive parameter while evaluating the energy spent on heating the water, no extra analysis is performed on this performance measure. However, for each scenario extra energy spent on heating the unreacted water is computed. It can be said that when the water is supplied to the system at stoichiometric ratio, most of the energy spent on heating the water, nearly 90-99% , is lost with the steam leaving the system for the non-zero efficiency cases in 4096 simulations. Table 4:9 shows amount of the energy loss percentage due to steam leaving the system for random selected scenarios.

**Table 4:9** Amount of the energy loss percentage due to steam leaving the system for random selected scenarios

| $Q_{water}$ (J) | $Q_{losswater}$ (J) | Loss Percentage (%) |
|---|---|---|
| 6973 | 6821 | 97.8 |
| 6973 | 6755 | 96.9 |
| 6973 | 6724 | 96.4 |
| 6973 | 6710 | 96.2 |
| 6973 | 6747 | 96.8 |
| 6973 | 6643 | 95.3 |
| 6973 | 6594 | 94.6 |
| 6973 | 6572 | 94.2 |
| 6973 | 6746 | 96.7 |
| 6973 | 6643 | 95.3 |

#### 4.3.1.7 Total Energy Supplied to the System

All of the factors are statistically important for the total energy supplied to the system as shown in Table 4:10.

**Table 4:10** Summary of the main effects and interactions for of total energy supplied to the system

| Source | Nparm | DF | Sum of Squares | F Ratio | Prob > F |
|---|---|---|---|---|---|
| Th | 1 | 1 | 494589888 | 20259.0 | <.0001* |
| DeltaT | 1 | 1 | 1548924409 | 63445.9 | <.0001* |
| Reduction Time 1 | 1 | 1 | 20466960.1 | 838.4 | <.0001* |
| Reduction Time 2 | 1 | 1 | 92500399.2 | 3788.9 | <.0001* |
| Oxidation Time 1 | 1 | 1 | 13235517.4 | 542.1 | <.0001* |
| Oxidation Time 2 | 1 | 1 | 27039134.2 | 1107.6 | <.0001* |
| Th*DeltaT | 1 | 1 | 572406.7 | 23.5 | <.0001* |
| Th*Reduction Time 1 | 1 | 1 | 5755524.2 | 235.8 | <.0001* |
| DeltaT*Reduction Time 1 | 1 | 1 | 40689.1 | 1.7 | 0.1969 |
| Th*Reduction Time 2 | 1 | 1 | 67342862.4 | 2758.5 | <.0001* |
| DeltaT*Reduction Time 2 | 1 | 1 | 308403.8 | 12.6 | 0.0004* |
| Reduction Time 1*Reduction Time 2 | 1 | 1 | 115.088115 | 0.0 | 0.9453 |
| Th*Oxidation Time 1 | 1 | 1 | 654491.5 | 26.8 | <.0001* |
| DeltaT*Oxidation Time 1 | 1 | 1 | 9675.9 | 0.4 | 0.5291 |
| Reduction Time 1*Oxidation Time 1 | 1 | 1 | 367.6 | 0.0 | 0.9024 |
| Reduction Time 2*Oxidation Time 1 | 1 | 1 | 13377.8 | 0.5 | 0.4592 |
| Th*Oxidation Time 2 | 1 | 1 | 19406874.6 | 794.9 | <.0001* |
| DeltaT*Oxidation Time 2 | 1 | 1 | 47046.7 | 1.9 | 0.1652 |
| Reduction Time 1*Oxidation Time 2 | 1 | 1 | 46549.1 | 1.9 | 0.1675 |
| Reduction Time 2*Oxidation Time 2 | 1 | 1 | 910180.5 | 37.3 | <.0001* |
| Oxidation Time 1*Oxidation Time 2 | 1 | 1 | 11246.5 | 0.5 | 0.4974 |
| Th*Th | 1 | 1 | 137849259 | 5646.4 | <.0001* |
| DeltaT*DeltaT | 1 | 1 | 6899.4 | 0.3 | 0.5951 |
| Reduction Time 1*Reduction Time 1 | 1 | 1 | 0.9 | 0.0 | 0.9952 |
| Reduction Time 2*Reduction Time 2 | 1 | 1 | 388.0 | 0.0 | 0.8997 |
| Oxidation Time 1*Oxidation Time 1 | 1 | 1 | 944.4 | 0.0 | 0.8441 |
| Oxidation Time 2*Oxidation Time 2 | 1 | 1 | 607581.7 | 24.9 | <.0001* |

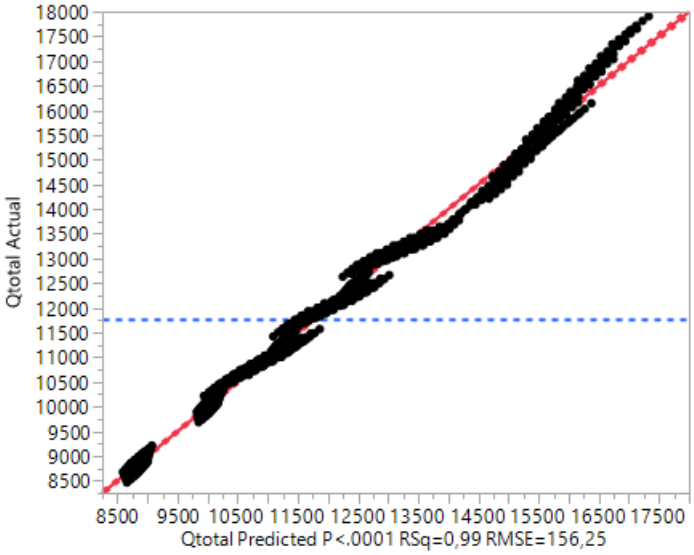


**Figure 4:18** Actual by predicted plot for of total energy supplied to the system

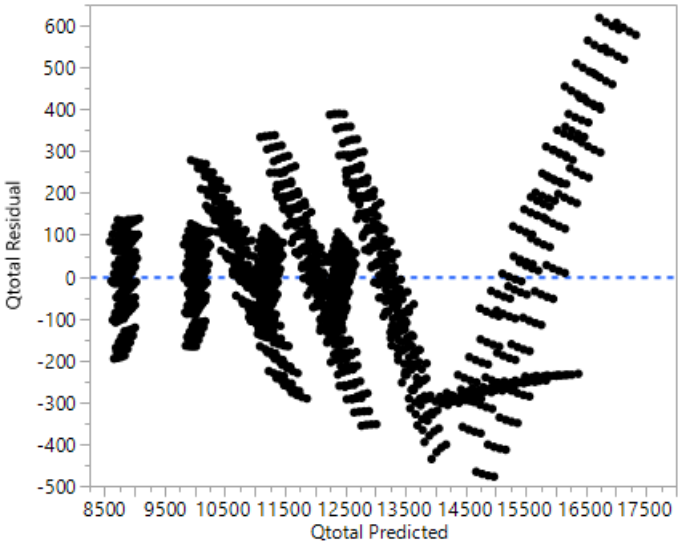


**Figure 4:19** Residual by predicted plot for of total energy supplied to the system

### 4.3.1.8 Optimized Values

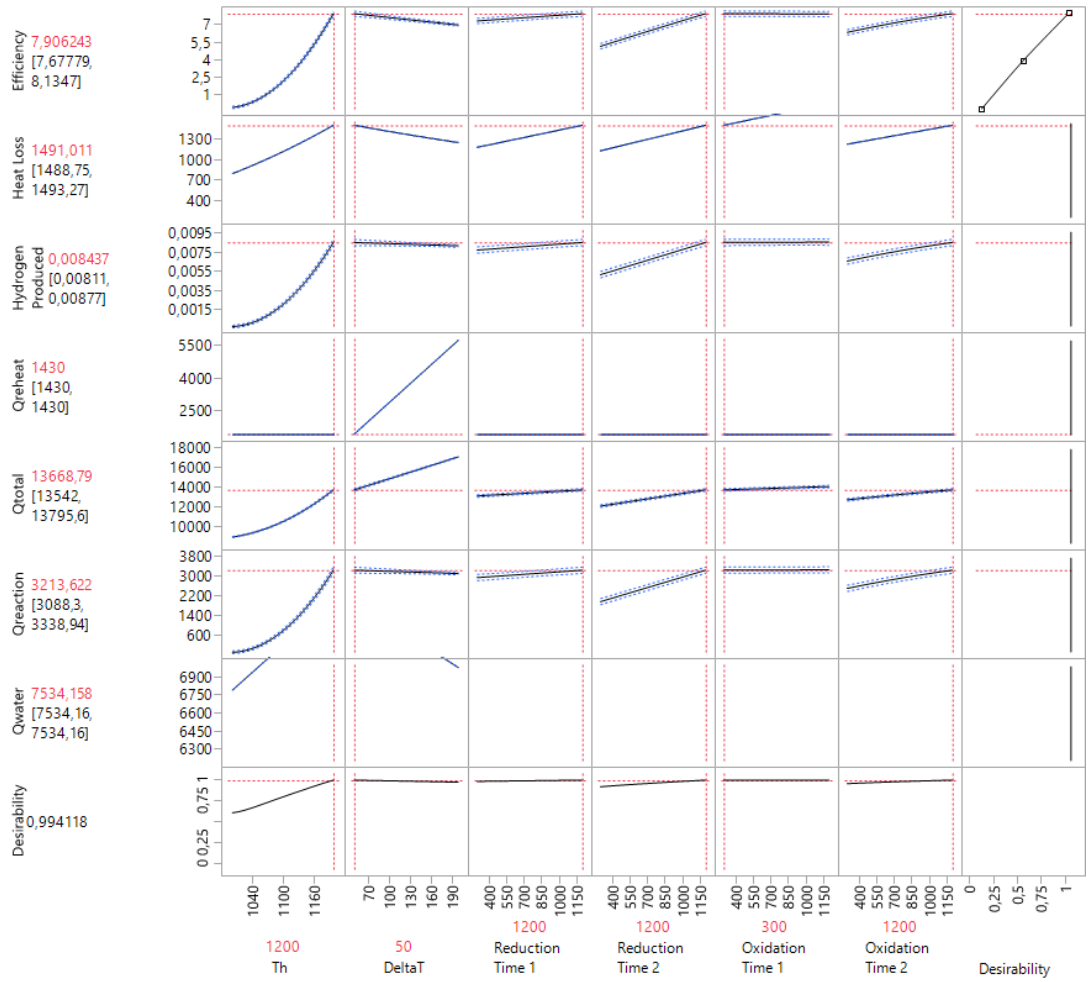


**Figure 4:20** Optimum values based on different performance measures

Based on Figure 4:20, optimum ranges for each factor can be specified as below:

- High reduction temperatures are desired to obtain higher total efficiencies.
- To maximize total efficiency, the temperature difference should be as low as possible.
- Reduction Time 1 and Oxidation Time 1 have less impact on the total efficiency than Reduction Time 2 and Oxidation Time 2. In other words, durations where the temperature is kept constant have more

effect on efficiency than durations where temperature increases linearly have.

- Longer durations are desirable for higher efficiencies except Oxidation Time 1. Since Oxidation Time 1 has no effect on efficiency statistically, minimum values for this factor are preferable to minimize heat loss.

### 4.3.2 Mathematical Optimization Method Results and Discussion

#### 4.3.2.1 Results and Discussion for Constant Temperature Conditions

For pre-selected operation duration values, local optimum working temperatures for reduction and oxidation phases are found by GAMS and tabulated in Table 4:11.

**Table 4:11** Results of optima temperatures for selected oxidation and reduction operation duration pairs obtained by solver SNOPT

| Duration Pair (s) | Reduction Temperature (K) | Oxidation Temperature (K) |
|---|---|---|
| 900-900 | 1050 | 1000 |
| 3600-3600 | 1050 | 1000 |
| 7200-3600 | 1070 | 905 |
| 3600-7200 | 1000 | 1050 |
| 7200-7200 | 1070 | 905 |

Moreover, the maximum values of the performance measure thermal efficiency combined by energy equivalent of hydrogen produced and components of energy supplied are shown in Table 4:12 for each corresponding optimum value of temperatures for the given oxidation and reduction durations.

**Table 4:12** Results of performance measures for selected duration pairs at evaluated process temperatures obtained by solver SNOPT

| Duration Pair (s) | Efficiency (%) | Amount of Hydrogen Produced (mol) | $Q_{total}$ (J) | $Q_{reheat}$ (J) | $Q_{rxn}$ (J) |
|---|---|---|---|---|---|
| 900-900 | 36.6 | 0.20 | 776100 | 1430 | 76180 |
| 3600-3600 | 36.6 | 0.20 | 776100 | 1430 | 76180 |
| 7200-3600 | 16.8 | 0.01 | 8580 | 4718.8 | 3861.3 |
| 3600-7200 | 36.6 | 0.20 | 776100 | 1430 | 76180 |
| 7200-7200 | 16.8 | 0.01 | 8580 | 4718.8 | 3861.3 |

**Table 4:13** Results of optima temperatures for selected oxidation and reduction operation duration pairs obtained by solver CONOPT

| Duration Pair (s) | Reduction Temperature (K) | Oxidation Temperature (K) |
|---|---|---|
| 900-900* | 1050 | 1000 |
| 3600-3600 | 1050 | 1000 |
| 7200-3600** | INFEASIBLE | INFEASIBLE |
| 3600-7200 | 1050 | 1000 |
| 7200-7200** | INFEASIBLE | INFEASIBLE |

*Loss of feasibility occurs while tightening tolerances

**Infeasible solution-no superbasic variables

**Table 4:14** Results of performance measures for selected duration pairs at evaluated process temperatures obtained by solver CONOPT

| Temperature Pair (K) | Efficiency (%) | Amount of Hydrogen Produced (mol) | $Q_{total}$ (J) | $Q_{reheat}$ (J) | $Q_{rxn}$ (J) |
|---|---|---|---|---|---|
| 900-900* | 29.5 | 0.01 | 6818.1 | 1430 | 5388.1 |
| 3600-3600 | 29.5 | 0.01 | 6827.3 | 1430 | 5397.3 |
| 7200-3600 | - | - | - | - | - |
| 3600-7200 | 31.9 | 0.02 | 9802 | 1430 | 8372 |
| 7200-7200** | - | - | - | - | - |

*Loss of feasibility occurs while tightening tolerances

**Infeasible solution-no superbasic variables

For same duration pairs model is also solved by using solver MINOS. However, all optimization runs evaluated by MINOS solver are infeasible.

# CHAPTER 5

# CONCLUSION

In this study, the objective is to evaluate the optimum operation temperatures and durations to achieve higher energy efficiencies in the solar thermochemical hydrogen production reactor. In the literature, there are several number of studies issued energy efficiency problem addressing the thermodynamic parametric analysis as solution way. However, thermodynamic analysis is not enough by itself to capture the true identity of efficiency of thermochemical cycle. Therefore, it is important to combine transient nature of the model, reaction kinetics, and dynamics for the solution of the problem. In this study, more than one solution approach is adopted in order to solve the problem. In the first approach, a parametric study based on statistical factorial analysis method is performed and the optimum values for the specific alternative scenarios are obtained. Statistically significant factors are determined for each performance measure. In the second approach, mathematical optimization method is applied to solve the efficiency problem model defined for constant temperature case. Optima values for the given durations are estimated for the nonlinear system

# CHAPTER 6

# FUTURE WORK

Future works are suggested for further analysis of the study. Further studies;

-Verification of the models can be done with experimental system results.

-Assumptions related dynamic optimization model can be relaxed to obtain more accurate results

- Two-step thermochemical water splitting system can be modeled as hybrid dynamic system and mixed integer dynamic optimization solution approach can be adopted for the solution of the problem.

- Dynamic optimization model should be investigated for transient behaviour. Section 6.1 gives information related to work done on the mathematical modelling of dynamic optimization problem.

## 6.1 Mathematical Formulation

### 6.1.1 Formulation of Dynamic Optimization Problem

In this part, only oxidation step of complex hybrid model consisting of two-step system is focused to optimize the operation temperature and duration during this step, due to the fact that energy efficiency problem is large and complex problem with many variables. A continuous time-dependent temperature optimization problem is modeled as below:

**Assumptions**

Following assumptions are done in order to determine the boundaries of the problem:

- Monolith reactor with one channel is considered for modeling.
- Inside of the channel of a monolith is a uniform system with no axial and radial changes in temperature or concentration of materials with respect to position
- First order reaction mechanism is assumed.
- Redox material properties and gas properties such as heat capacities are constant.
- Gas flow is laminar.
- Pressure throughout the monolith channel is constant, since pressure drop is small in the channel and it can be neglected.

**Performance Measure**

$$\int_0^{t_f} [\alpha_1 (T_H - T(t)) + \alpha_2 \left(n_{H_{2,max}} - n_{H_2}(t)\right)] \, dt \qquad (6.1)$$

where $\alpha_1 \; and \; \alpha_2$ are weights of the objectives.

**Decision Variables**

Oxidation temperature and amount of the hydrogen produced are the two decision variables for the specified system.

**Constraints**

1. **Constraints on reaction kinetics:**

Equations 3.7 and 3.8 are used as constraints for reactions kinetics.

2. **Constraints on reactor dynamics:**

$$\frac{dT}{dt} = \frac{\dot{Q}_{Loss(ox)} + A \cdot \Delta H_f \cdot r_{wsp}}{A \cdot r_{wsp} \cdot c_{p,H_2} + \dot{n}_{H_2O} c_{p,H_2O} + \dot{n}_{RM} c_{p,RM}} \qquad (6.2)$$

3. **Bounds on oxidation temperature:**

$$T_H \leq T \leq T_{allowable} \tag{6.3}$$

## REFERENCES


[1] H. Cavendish, “Three Papers , Containing Experiments on Factitious Air,” *Philos. Trans.*, vol. 56, pp. 141–184, 1766.

[2] J. A. Turner, M. C. Williams, and K. Rajeshwar, “Hydrogen Economy based on Renewable Energy Sources,” *Electrochem. Soc. Interface*, vol. 13, pp. 24–30, 2004.

[3] I. Dincer and C. Acar, “Review and evaluation of hydrogen production methods for better sustainability,” *Int. J. Hydrogen Energy*, vol. 40, no. 34, pp. 11094–11111, 2014.

[4] A. Bakenne, W. Nuttall, and N. Kazantzis, “Sankey-Diagram-based insights into the hydrogen economy of today,” *Int. J. Hydrogen Energy*, vol. 41, no. 19, pp. 7744–7753, 2015.

[5] G. Marbán and T. Valdés-Solís, “Towards the hydrogen economy?,” *Int. J. Hydrogen Energy*, vol. 32, no. 12, pp. 1625–1637, 2007.

[6] C. Acar and I. Dincer, “Impact assessment and efficiency evaluation of hydrogen production methods,” *Int. J. Energy Res.*, vol. 39, no. 13, pp. 1757–1768, 2015.

[7] International Energy Agency, “Energy and Air Pollution,” 2016.

[8] International Energy Agency, “Energy and Climate Change,” 2015.

[9] International Energy Agency, “Key Renewables Trends: Statistics,” 2016.

[10] L. Vayssieres, *On Solar Hydrogen & Nanotechnology*. 2010.

[11] A. Steinfeld, “Solar thermochemical production of hydrogen—a review,” *Sol. Energy*, vol. 78, no. 5, pp. 603–615, 2005.

[12] A. Kogan, “Direct solar thermal splitting of water and on-site separation of the products-II. Experimental feasibility study,” *Int. J. Hydrogen Energy*, vol. 23, no. 2, pp. 89–98, 1998.

[13] A. Ozbilen, I. Dincer, and M. A. Rosen, “A comparative life cycle analysis of hydrogen production via thermochemical water splitting using a Cu-Cl cycle,” *Int. J. Hydrogen Energy*, vol. 36, no. 17, pp. 11321–11327, 2011.

[14] G. J. Kolb and R. B. Diver, “Screening Analysis of Solar Thermochemical Hydrogen Concepts,” 2008.

[15] T. Nakamura, “Hydrogen production from water utilizing solar heat at high temperatures,” *Sol. Energy*, vol. 19, no. 5, pp. 467–475, 1977.

[16] C. Acar, S. Ghosh, I. Dincer, and C. Zamfirescu, “Evaluation of a new continuous type hybrid photo-electrochemical system,” *Int. J. Hydrogen Energy*, vol. 40, no. 34, pp. 11112–11124, 2015.

[17] C. J. Winter, “The hydrogen energy economy: an address to the World Economic Forum 2004,” *Int. J. Hydrogen Energy*, vol. 29, no. 11, pp. 1095–1097, 2004.

[18] W. C. Chueh and S. M. Haile, “A thermochemical study of ceria: exploiting an old material for new modes of energy conversion and CO2 mitigation,” *Philos. Trans. R. Soc. A Math. Phys. Eng. Sci.*, vol. 368, no. 1923, pp. 3269–3294, 2010.

[19] P. Charvin, S. Abanades, G. Flamant, and F. Lemort, “Two-step water splitting thermochemical cycle based on iron oxide redox pair for solar hydrogen production,” *Energy*, vol. 32, no. 7, pp. 1124–1133, 2007.

[20] D. Yadav and R. Banerjee, “A review of solar thermochemical processes,” *Renew. Sustain. Energy Rev.*, vol. 54, pp. 497–532, 2016.

[21] J. Chen, H. Yang, N. Wang, Z. Ring, and T. Dabros, “Mathematical modeling of monolith catalysts and reactors for gas phase reactions,” *Applied Catalysis*

*A: General*, vol. 345, no. 1. pp. 1–11, 2008.

[22] A. Patton, B. D. Crittenden, and S. P. Perera, “Use of the Linear Driving Force Approximation to Guide the Design of Monolithic Adsorbents,” *Chem. Eng. Res. Des.*, vol. 82, no. 8, pp. 999–1009, 2004.

[23] M. Roeb, C. Sattler, R. Klüser, N. Monnerie, L. de Oliveira, A. G. Konstandopoulos, C. Agrafiotis, V. T. Zaspalis, L. Nalbandian, A. Steele, and P. Stobbe, “Solar Hydrogen Production by a Two-Step Cycle Based on Mixed Iron Oxides,” *J. Sol. Energy Eng.*, vol. 128, no. 2, p. 125, 2006.

[24] L. C. Young and B. A. Finlayson, “Mathematical Models of the Monolith Converter,” *AIChE J.*, vol. 22, no. 2, pp. 331–344, 1976.

[25] C. Agrafiotis, M. Roeb, A. G. Konstandopoulos, L. Nalbandian, V. T. Zaspalis, C. Sattler, P. Stobbe, and A. M. Steele, “Solar water splitting for hydrogen production with monolithic reactors,” in *Solar Energy*, 2005, vol. 79, no. 4, pp. 409–421.

[26] J. Dersch, A. Mathijsen, M. Roeb, and C. Sattler, “Modelling of a solar thermal reactor for hydrogen generation,” *5th Int. Model.*, pp. 441–448, 2006.

[27] C. C. Agrafiotis, C. Pagkoura, S. Lorentzou, M. Kostoglou, and A. G. Konstandopoulos, “Hydrogen production in solar reactors,” *Catal. Today*, vol. 127, no. 1–4, pp. 265–277, 2007.

[28] J. Petrasch, P. Osch, and A. Steinfeld, “Dynamics and control of solar thermochemical reactors,” *Chem. Eng. J.*, vol. 145, no. 3, pp. 362–370, 2009.

[29] M. Kostoglou, C. P. Lekkos, and A. G. Konstandopoulos, “On mathematical modeling of solar hydrogen production in monolithic reactors,” *Comput. Chem. Eng.*, vol. 35, no. 9, pp. 1915–1922, 2011.

[30] P. Furler and A. Steinfeld, “Heat transfer and fluid flow analysis of a 4kW solar thermochemical reactor for ceria redox cycling,” *Chem. Eng. Sci.*, vol. 137, pp. 373–383, 2015.

[31] M. Lange, M. Roeb, C. Sattler, and R. Pitz-Paal, “Efficiency assessment of a two-step thermochemical water-splitting process based on a dynamic process model,” *Int. J. Hydrogen Energy*, vol. 40, no. 36, pp. 12108–12119, 2015.

[32] C. Yuan, C. Jarrett, W. Chueh, Y. Kawajiri, and A. Henry, “A new solar fuels reactor concept based on a liquid metal heat transfer fluid: Reactor design and efficiency estimation,” *Sol. Energy*, vol. 122, pp. 547–561, 2015.

[33] M. Lange, M. Roeb, C. Sattler, and R. Pitz-Paal, “T-S diagram efficiency analysis of two-step thermochemical cycles for solar water splitting under various process conditions,” *Energy*, vol. 67, pp. 298–308, 2014.

[34] I. Dinçer and M. (Marc A. . Rosen, *Exergy : energy, environment, and sustainable development*. Elsevier, 2007.

[35] D. Yadav and R. Banerjee, “A review of solar thermochemical processes,” *Renew. Sustain. Energy Rev.*, vol. 54, pp. 497–532, 2016.

[36] W. C. Chueh, C. Falter, M. Abbott, D. Scipio, P. Furler, S. M. Haile, and A. Steinfeld, “High-flux Solar-driven Thermochemical Dissociation of $CO_2$ and $H_2O$ Using Nonstoichiometric Ceria.,” *Science*, vol. 330, no. 6012, pp. 1797–801, 2010.

[37] R. B. Diver, J. E. Miller, M. D. Allendorf, N. P. Siegel, and R. E. Hogan, “Solar Thermochemical Water-Splitting Ferrite-Cycle Heat Engines,” *J. Sol. Energy Eng.*, vol. 130, no. 4, p. 041001, 2008.

[38] P. Charvin, A. St??phane, L. Florent, and F. Gilles, “Analysis of solar chemical processes for hydrogen production from water splitting thermochemical cycles,” *Energy Convers. Manag.*, vol. 49, no. 6, pp. 1547–1556, 2008.

[39] J. R. Scheffe and A. Steinfeld, “Thermodynamic analysis of cerium-based oxides for solar thermochemical fuel production,” *Energy and Fuels*, vol. 26, no. 3, pp. 1928–1936, 2012.

[40] L. J. Venstrom, M. Robert, M. Sossina, and H. Jane, “Efficient Splitting of

CO2 in an Isothermal Redox Cycle Based on Ceria," vol. 28 SRC -, pp. 2732–2742, 2014.

[41] J. Lapp, J. H. Davidson, and W. Lipinski, "Efficiency of two-step solar thermochemical non-stoichiometric redox cycles with heat recovery," *Energy*, vol. 37, no. 1, pp. 591–600, 2012.

[42] N. P. Siegel, J. E. Miller, I. Ermanoski, R. B. Diver, and E. B. Stechel, "Factors affecting the efficiency of solar driven metal oxide thermochemical cycles," *Ind. Eng. Chem. Res.*, vol. 52, no. 9, pp. 3276–3286, 2013.

[43] R. Bader, L. J. Venstrom, J. H. Davidson, and W. Lipinski, "Thermodynamic analysis of isothermal redox cycling of ceria for solar fuel production," *Energy and Fuels*, vol. 27, no. 9, pp. 5533–5544, 2013.

[44] I. Ermanoski, N. P. Siegel, and E. B. Stechel, "A New Reactor Concept for Efficient Solar-Thermochemical Fuel Production," *J. Sol. Energy Eng.*, vol. 135, no. 3, p. 031002, 2013.

[45] I. Ermanoski, J. E. Miller, and M. D. Allendorf, "Efficiency maximization in solar-thermochemical fuel production: challenging the concept of isothermal water splitting.," *Phys. Chem. Chem. Phys.*, vol. 16, no. 18, pp. 8418–8427, 2014.

[46] I. Ermanoski, "Maximizing Efficiency in Two-step Solar-thermochemical Fuel Production," *Energy Procedia*, vol. 69, pp. 1731–1740, 2015.

[47] J. E. Miller, A. Ambrosini, E. N. Coker, M. D. Allendorf, and A. H. McDaniel, "Advancing oxide materials for thermochemical production of solar fuels," *Energy Procedia*, vol. 49, pp. 2019–2026, 2014.

[48] S. Tescari, N. Mazet, and P. Neveu, "Constructal method to optimize solar thermochemical reactor design," *Sol. Energy*, vol. 84, no. 9, pp. 1555–1566, 2010.

[49] L. D'Souza, "Thermochemical hydrogen production from water using

reducible oxide materials: a critical review," *Mater. Renew. Sustain. Energy*, vol. 2, no. 1, p. 7, 2013.

[50] S. Abanades, P. Charvin, G. Flamant, and P. Neveu, "Screening of water-splitting thermochemical cycles potentially attractive for hydrogen production by concentrated solar energy," *Energy*, vol. 31, no. 14, pp. 2469–2486, 2006.

[51] M. Lundberg, "Model calculations on some feasible two-step water splitting processes," *Int. J. Hydrogen Energy*, vol. 18, no. 5, pp. 369–376, 1993.

[52] A. Steinfeld, "Solar hydrogen production via a two-step water-splitting thermochemical cycle based on Zn/ZnO redox reactions," *Int. J. Hydrogen Energy*, vol. 27, no. 6, pp. 611–619, 2002.

[53] A. Segal and M. Epstein, "Optimized working temperatures of a solar central receiver," *Sol. Energy*, vol. 75, no. 6, pp. 503–510, 2003.

[54] A. Salome, F. Chhel, G. Flamant, A. Ferriere, and F. Thiery, "Control of the flux distribution on a solar tower receiver using an optimized aiming point strategy: Application to THEMIS solar tower," *Sol. Energy*, vol. 94, pp. 352–366, 2013.

[55] L. Roca, R. Diaz-Franco, A. de la Calle, J. Bonilla, and A. Vidal, "A control based on a knapsack problem for solar hydrogen production," *Optim. Control Appl. METHODS*, 2014.

[56] M. Sturzenegger and P. Nüesch, "Efficiency analysis for a manganese-oxide-based thermochemical cycle," *Energy*, vol. 24, no. 11, pp. 959–970, 1999.

[57] A. Houaijia, C. Sattler, M. Roeb, M. Lange, S. Breuer, and J. P. Säck, "Analysis and improvement of a high-efficiency solar cavity reactor design for a two-step thermochemical cycle for solar hydrogen production from water," *Sol. Energy*, vol. 97, pp. 26–38, 2013.

[58] I. Ermanoski, "Cascading pressure thermal reduction for efficient solar fuel production," *Int. J. Hydrogen Energy*, vol. 39, no. 25, pp. 13114–13117, 2014.

[59] C. Jarrett, W. Chueh, C. Yuan, Y. Kawajiri, K. H. Sandhage, and A. Henry, "Critical limitations on the efficiency of two-step thermochemical cycles," *Sol. Energy*, vol. 123, pp. 57–73, 2016.

[60] D. J. Keene, J. H. Davidson, and W. Lipiński, "A Model of Transient Heat and Mass Transfer in a Heterogeneous Medium of Ceria Undergoing Nonstoichiometric Reduction," *J. Heat Transfer*, vol. 135, no. 5, p. 052701, 2013.

[61] J. Lapp and W. Lipiński, "Transient Three-Dimensional Heat Transfer Model of a Solar Thermochemical Reactor for $H_2O$ and $CO_2$ Splitting Via Nonstoichiometric Ceria Redox Cycling," *J. Sol. Energy Eng.*, vol. 136, no. 3, p. 031006, 2014.

[62] R. Bala Chandran, R. Bader, and W. Lipiński, "Transient heat and mass transfer analysis in a porous ceria structure of a novel solar redox reactor," *Int. J. Therm. Sci.*, vol. 92, pp. 138–149, 2015.

[63] M. E. Huntelaar, A. S. Booij, E. H. P. Cordfunke, R. R. van der Laan, A. C. G. van Genderen, and J. C. van Miltenburg, "The thermodynamic properties of Ce2O3(s) fromT→ 0 K to 1500 K," *J. Chem. Thermodyn.*, vol. 32, no. 4, pp. 465–482, 2000.

[64] S. S. Rao, *Engineering Optimization Theory and Practice Fourth Edition*. 2009.

[65] L. T. Biegler, *Nonlinear Programming: Concepts, Algorithms, and Applications to Chemical Processes*. 2010.

[66] A. Cervantes and L. T. Biegler, "Optimization strategies for dynamic systems Optimization Strategies for Dynamic Systems," in *Encyclopedia of Optimization*, A. C. Floudas and M. P. Pardalos, Eds. Boston, MA: Springer US, 2009, pp. 2847–2858.

[67] Y. Zhu, "Efficient Nonlinear Optimization With Rigorous Models for Large

Scale Industrial Chemical Processes," no. May, 2011.

[68] T. J. Berna, M. H. Locke, and A. W. Westerberg, "New Approach To Optimization of Chemical Processes," *Aiche J.*, vol. 26, no. 1, pp. 37–43, 1980.

[69] D. Aksen, *The Complete Reference for the General Algebraic Modeling System GAMS: Teach Yourself GAMS*. Boğaziçi University Press, 1998.

# APPENDIX A

## MATLAB CODE FOR PARAMETRIC ANALYSIS

TWO-STEP THERMOCHEMİCAL WATER SPLITTING SYSTEM
A PARAMETRIC STUDY

```
[~, ~, raw] =
xlsread('C:\Users\MONSTER\Documents\MATLAB\func.xlsx','Sayfa1','A2:F4097');
A = reshape([raw{:}],size(raw));
clearvars raw;
M=zeros(4096,10);

for k=1:4096
Th=A(k,1);
DeltaT=A(k,2);
tau1 = A(k,3);
tau2 = A(k,4);
tau3 = A(k,5);
tau4 = A(k,6);
[therm_eff, Qloss, n_H2total, Qreheat,Qtotal, Qrxn,
Qwater,Qlosswater,n_O2total,n_H2old]=func(Th,DeltaT,tau1,tau2,tau3,tau4) ;
M(k,:)=[therm_eff, Qloss, n_H2total, Qreheat,Qtotal, Qrxn,
Qwater,Qlosswater,n_O2total,n_H2old];
end
filename='results.xlsx';
xlswrite(filename,M,'Sayfa1')
```

```
function [therm_eff, Qloss, n_H2total, Qreheat,Qtotal, Qrxn,
Qwater,Qlosswater,n_O2total, n_H2old]=func(Th,DeltaT,tau1,tau2,tau3,tau4)

%Operating Conditions
Tc=Th-DeltaT ;          %water splitting temperature in K
P_H2O=1e5;              %partial pressure of water in feed in Pa
R = 8.314      ;        %Gas constant in J/mol/K
c_H2O=P_H2O/(R*Tc) ;    %Concentration of water in the feed in mol/m^3
Ta=298     ;            %Ambient air temperature in K
alpha1=(Th-Tc)/tau1;
alpha2=(Th-Tc)/tau3;
tau=[tau1 tau2 tau3 tau4]    %time period of each step
CycleTime= sum(tau) ;   %Cycle time
```

```
ReductionTime= tau1 +tau(2); %reduction time
OxidationTime=tau3 +tau(4); % oxidation time
t0=0 ;                  %initial value

%Design parameters
ntotal=0.1         ;    %maximum(allowable) storage capacity of wall in mol/m^2
rec_s=0             ;   %fraction of heat recuperation in solid
n_CeO2=0.2           ;  %number of moles of CeO2 loaded
A=1                   ; %Area of monolith channel in m^2
Ar=3.14E-6           ;%Effective Surface area where the heat loss occurs(monolith
outerface)

%Material Parameters
kc_red=1000000 ;          %rate constant of Arrhenius in redcution step in s^-1
kc_wsp=35     ;         %rate constant of Arrhenius in water splitting step in
m^3/mol/s
Ea_red=240000  ;        %Activation energy of reduction step in J/mol
Ea_wsp=100000     ;       %Activation energy of oxidation step in J/mol
cp_solid=143     ;      %heat capacity of redox material in J/mol/K
deltaHred=380900     ;     %enthalpy change in reduction of redox material in J/mol
HHV=142180         ;    %higher heating value of hydrogen in J/mol
h=20            ;   %Convective heat transfer coefficient in W/m^2/K
cpwater=37.4 ;        %heat capacity of steam

%Constants
R = 8.314      ;        %Gas constant in J/mol/K
sigma=5.670373E-8  ;    %Stefan-Boltzmann Constant in W/m^2/K^4


%Section 1
    y0=1;
    [t, y] = ode45(@(t,y) reduction1(t,y,alpha1,Tc,tau1,kc_red,Ea_red,R,A),[t0
tau1],y0);
    qr1=@(t)Ar*sigma*((alpha1*t +Tc).^4-Ta.^4);
    qr10=0;
    Qrad(1)= integral(qr1,t0,tau(1));
    qc1=@(t)Ar*h*((alpha1*t +Tc)-Ta);
    Qconv(1)= integral(qc1,t0,tau(1));

    dim=size(y);
    n_O21=(1- y(dim(1)))*ntotal;

    %Section 2 Adsorption
    y10=y(dim(1));
    [t1, y1]=ode45(@(t1,y1)reduction2(t1,y1,kc_red,Ea_red,R,Th,A),[tau1
tau(2)+tau1],y10);
    Qrad(2)= Ar*sigma*(Th.^4-Ta.^4)*(tau(2)-t0);
    Qconv(2)= Ar*h*(Th-Ta)*(tau(2)-t0);
    dim1=size(y1);
    n_O22=(y(dim(1))- y1(dim1(1)))*ntotal;
```

```
n_O2total=n_O21+n_O22;
%Section 3 Cooling
    y20=y1(dim1(1));
    p=tau1+tau(2);
    [t2,y2]=ode45(@(t2,y2)
oxidation1(t2,y2,kc_wsp,Ea_wsp,R,Th,alpha2,c_H2O,A,p),[tau1+tau(2)
tau(2)+tau1+tau3],y20);
    qr3=@(t)Ar*sigma*((Th-alpha2*t).^4-Ta.^4);
    qr30=0;
    Qrad(3)= integral(qr3,t0,tau(3));
    qc3=@(t)Ar*h*((Th-alpha2*t)-Ta);
    Qconv(3)= integral(qc3,t0,tau(3));
    dim2=size(y2);
    n_H21= 2*(y2(dim2(1))-y1(dim(1)))*ntotal ;
%    for i=1:dim2;
%      if  y2(i)<=1

%Section 4 Adsorption

    y30=y2(dim2(1));

[t3,y3]=ode45(@(t3,y3)oxidation2(t3,y3,kc_wsp,Ea_wsp,R,Tc,c_H2O,A),[tau3+tau(2)+tau1
tau(2)+tau1+tau3+tau(4)],y30);
    Qrad(4)=  Ar*sigma*(Tc^4-Ta.^4)*(tau(4)-t0);
    Qconv(4)= Ar*h*(Tc-Ta)*(tau(4)-t0);
    dim3=size(y3);
    n_H22=2* (y3(dim3(1))-y2(dim(1)))*ntotal;
    for j=1:dim3;
    if y3(j)>=1;
        display "error"
   end
%     end

    figure(2);

    plot(t,y,t1,y1,t2,y2,t3,y3)

%      else
%          break;
%     end
  end
n_H2total=n_H21+n_H22;
n_H2old=n_H2total;
if n_H2total/2>n_O2total;
     n_H2total=n_O2total*2;
    display "excess"
end
Qloss=Qrad(1)+Qconv(1)+Qrad(2)+Qconv(2)+Qrad(3)+Qconv(3)+Qrad(4)+Qconv(4);

nH2O=n_CeO2/2;
Qlosswater=(nH2O-n_H2total)*((cpwater*(Tc-373))+46281.78);
```

```
Qwater=nH2O*((cpwater*(Tc-373))+46281.78 );
Qreheat = ((1-rec_s)*n_CeO2*cp_solid*(Th-Tc)) ;
Qrxn = n_H2total*deltaHred           ;
Qtotal = Qreheat+Qrxn + Qloss +Qwater;
en_hyd = n_H2total*HHV            ;
therm_eff =100* en_hyd /(Qtotal) ;

end
```

```
function dydt=reduction1(t,y,alpha1,Tc,tau1,kc_red,Ea_red,R,A)
T =alpha1*t +Tc ;
figure(1);
hold on
plot(t,T,'o')
hold off
  Tk = alpha1*tau1 +Tc ;
  if T>=1000 && T<Tk;
     dydt=-A*kc_red*exp((-Ea_red)/(R*(alpha1*t +Tc)))*(y);
 else
    dydt=0;
 end
end
```

```
function dydt=reduction2(t1,y1,kc_red,Ea_red,R,Th,A)
figure(1);
hold on
plot(t1,Th,'*')
hold off
if Th>=1000
k_red2 =-A*kc_red *exp((-Ea_red)/(R*Th));
    dydt= k_red2*(y1);
else
    dydt=0;
end
end
```

```
function dydt=oxidation1(t2,y2,kc_wsp,Ea_wsp,R,Th,alpha2,c_H2O,A,p)
T1=Th-alpha2*(t2-p);
figure(1);
hold on
plot(t2,T1,'o')
hold off
if T1<=1000;
 dydt=A*kc_wsp*exp((-Ea_wsp)/(R*(Th-alpha2*(t2-p))))*c_H2O*(1-y2);
else
    dydt=0;
end
end
```

```
function dydt=oxidation2(t3,y3,kc_wsp,Ea_wsp,R,Tc,c_H2O,A)
figure(1);
hold on
```

```
plot(t3,Tc,'*')
hold off
if Tc<=1000
k_wsp2= kc_wsp*exp((-Ea_wsp)/(R*Tc));
dydt=A*k_wsp2*c_H2O*(1-y3);
else
    dydt=0;
end
end
```

*Published with MATLAB® R2016a*

# APPENDIX B

## GAMS CODE FOR TEMPERATURE OPTIMIZATION IN DISCRETIZED SYSTEM FOR STEADY-STATE CONDITIONS

```
$Ontext
A programme to adjust the temperatures between two-step solar
thermochemical
splitting cycle steps
$Offtext


Sets
i " number of periods" /1*2/
Parameters
tau(i)    "time required for reduction period"  /(1)=7200, (2)=7200/
ntotal    "maximum storage capacity of wall in mol/m^2" /0.1/
HHV       "higher heating value of hydrogen in J/mol" /142180/
deltaH    "enthalpy change in reduction of redox material in J/mol"
/380900/
rec_s     "fraction of heat recuperation in solid" /0/
cp_solid "heat capacity of redox material in J/mol/K" /143/
n_CeO2    "number of moles of CeO2"  /0.2/
kc_red    "rate constant of Arrhenius in redcution step in s^-1"
/10E6/
kc_wsp    "rate constant of Arrhenius in water splitting step in
m^3/mol/s" /35/
Ea_red    "Activation energy of reduction step in J/mol" /240000/
Ea_wsp    "Activation energy of oxidation step in J/mol" /10E5/
R         "Gas constant in J/mol/K" /8.314/
A         "Area of monolith channel in m^2" /1/
Ta        "ambient temperature" /298/
P_H2O      "Partial pressure of water in feed" /100000/ ;

positive variables
Th        "reduction temperature in K"
Tc        "water splitting temperature in K"

n_H2      "amount of hydrogen produced at the end of the complete
```

```
cycle"
n_O2      "amount of oxygen release at the end of the reduction
step"
en_hyd    "energy of produced hydrogen"
Qtotal    "Total energy amount supplied to the system"
Qreheat   "energy required to reheat the system from Tc to Th"
Qrxn      "energy required for endothermic reaction"
B_red     "Conctants for reduction step for surface  coverage"
B_wsp     "Constants for water splitting step for surface coverage"
k_red     "rate constant of reduction reaction"
k_wsp     "rate constant of water splitting step"
y(i)      "fraction of the surface coverage at the end of period i";

Free Variables
therm_eff "objective function" ;

Equations
obj
eqn1
eqn2
eqn3
eqn4
eqn10
eqn11
eqn12
eqn13
eqn14(i)
eqn15(i)
eqn16(i)
eqn17(i)
eqn18
eqn20;

obj..en_hyd=e=therm_eff*(Qtotal) ;
eqn1..n_H2*HHV =e=en_hyd ;
eqn2..Qreheat+Qrxn =e= Qtotal;
eqn3..((1-rec_s)*n_CeO2*cp_solid*(Th-Tc)) =e= Qreheat ;
eqn4..n_H2* deltaH =e= Qrxn ;
eqn10..kc_red*exp((-Ea_red)/(R*Th)) =e= k_red ;
eqn11..kc_wsp*exp((-Ea_wsp)/(R*Tc)) =e= k_wsp ;
eqn12..A*k_red =e= B_red ;
eqn13..A*k_wsp*P_H2O =e= B_wsp ;
eqn14(i)..exp((-1)*B_red*tau('1')) =e= y('1') ;
eqn15(i)..( 1-y('1'))*ntotal =e= n_O2;
eqn16(i)..exp((-1)*B_wsp*tau('2'))=e= y('2');
eqn17(i)..(1-y('2'))*ntotal*2=e= n_H2  ;
eqn18..y('2')=l=y('1');
eqn20..n_O2=l=ntotal ;

Th.l=1200;
```

```
Tc.l=900;
Tc.up=1000;
Th.lo=1050;
Th.up=1200;
Tc.lo=900;

Model rawmodel1 /all/;

solve rawmodel1 maximize therm_eff using nlp;
option decimals=8;
display therm_eff.L,y.L,B_red.L,B_wsp.L,k_red.L,
k_wsp.L,Tc.L,Th.L,n_H2.L, n_H2.M,n_O2.M,n_O2.L, Qreheat.L, Qrxn.L;
```